



**HAL**  
open science

## Late Smithian microbial deposits and their lateral marine fossiliferous limestones (Early Triassic, Hurricane Cliffs, Utah, USA)

Nicolas Olivier, Emmanuel Fara, Emmanuelle Vennin, Kevin Bylund, James Jenks, Gilles Escarguel, Daniel A. Stephen, Nicolas Goudemand, Dawn Snyder, Christophe Thomazo, et al.

### ► To cite this version:

Nicolas Olivier, Emmanuel Fara, Emmanuelle Vennin, Kevin Bylund, James Jenks, et al.. Late Smithian microbial deposits and their lateral marine fossiliferous limestones (Early Triassic, Hurricane Cliffs, Utah, USA). *Facies*, 2018, 64 (2), pp.13. 10.1007/s10347-018-0526-3 . hal-01748441

**HAL Id: hal-01748441**

**<https://uca.hal.science/hal-01748441>**

Submitted on 10 Dec 2019

**HAL** is a multi-disciplinary open access archive for the deposit and dissemination of scientific research documents, whether they are published or not. The documents may come from teaching and research institutions in France or abroad, or from public or private research centers.

L'archive ouverte pluridisciplinaire **HAL**, est destinée au dépôt et à la diffusion de documents scientifiques de niveau recherche, publiés ou non, émanant des établissements d'enseignement et de recherche français ou étrangers, des laboratoires publics ou privés.

[Click here to view linked References](#)

1 **Late Smithian microbial deposits and their lateral marine fossiliferous limestones (Early**  
2 **Triassic, Hurricane Cliffs, Utah, USA)**

3  
4 Nicolas Olivier<sup>1</sup> · Emmanuel Fara<sup>2</sup> · Emmanuelle Vennin<sup>2</sup> · Kevin G. Bylund<sup>3</sup> · James F.  
5 Jenks<sup>4</sup> · Gilles Escarguel<sup>5</sup> · Daniel A. Stephen<sup>6</sup> · Nicolas Goudemand<sup>7</sup> · Dawn Snyder<sup>8</sup> · C.  
6 Thomazo<sup>2</sup> · Arnaud Brayard<sup>2</sup>

7  
8  
9 <sup>1</sup>*Université Clermont Auvergne, CNRS, Laboratoire Magmas et Volcans, F-63000 Clermont-Ferrand, France*

10 <sup>2</sup>*Biogéosciences, UMR 6282, CNRS, Université Bourgogne Franche-Comté, 6 Boulevard Gabriel, 21000 Dijon,*

11 *France*

12 <sup>3</sup>*140 South 700 East, Spanish Fork, Utah 84660, USA*

13 <sup>4</sup>*1134 Johnson Ridge Lane, West Jordan, Utah 84084, USA*

14 <sup>5</sup>*Université de Lyon, Laboratoire d'Ecologie des Hydrosystèmes Naturels et Anthropisés, UMR CNRS 5023,*

15 *Université Claude Bernard Lyon 1, ENTPE, 6 rue Raphaël Dubois, F-69622 Villeurbanne, France*

16 <sup>6</sup>*Utah Valley University, Department of Earth Science, Orem, Utah 84058, USA*

17 <sup>7</sup>*Université de Lyon, ENS de Lyon, CNRS, Université Claude Bernard Lyon 1, Institut de Génomique*

18 *Fonctionnelle de Lyon, UMR 5242, 46 Allée d'Italie, F-69364 Lyon cedex 07, France*

19 <sup>8</sup>*7202 Yardley Drive, Katy Texas 77494, USA*

20  
21 Corresponding author: nicolas.olivier@uca.fr

22

23

24  
25 **Abstract**

26 Recurrent microbialite proliferations during the Early Triassic are usually explained  
27 by ecological relaxation and abnormal oceanic conditions. Most Early Triassic microbialites  
28 are described as single or multiple lithological units without detailed ecological information  
29 about lateral and coeval fossiliferous deposits. Exposed rocks along Workman Wash in the  
30 Hurricane Cliffs (south-western Utah, USA) provide an opportunity to reconstruct the spatial  
31 relationships of late Smithian microbialites with adjacent and contemporaneous fossiliferous  
32 sediments. Microbialites deposited in an intertidal to subtidal interior platform, are  
33 intercalated between inner tidal flat dolosiltstones and subtidal bioturbated fossiliferous  
34 limestones. Facies variations along these fossiliferous deposits and microbialites can be traced  
35 laterally over a few hundred of meters. Preserved organisms reflect a moderately diversified  
36 assemblage, contemporaneous to the microbialite formation. The presence of such a fauna,  
37 including some stenohaline organisms (echinoderms) indicates that the development of these  
38 late Smithian microbial deposits occurred in normal marine waters as a simple facies belt  
39 subject to relative sea-level changes. Based on this case study, the proliferation of

40 microbialites cannot be considered as direct evidence for presumed harsh environmental  
41 conditions.

42

43 **Keywords** Early Triassic · Late Smithian · Microbial deposits · Metazoan fauna · Lingulids ·  
44 Biotic recovery · Depositional environments

45

46

## 47 **1. Introduction**

48         The biotic recovery after the Permian-Triassic mass extinction is usually considered to  
49 have lasted as long as the entire Early Triassic (Erwin 2001; Flügel 2002). The patterns and  
50 causes of this delayed recovery are strongly debated, and possibly involve environmental,  
51 ecological and preservational factors (Erwin 1996; Payne and Clapham 2012; Pietsch et al  
52 2014; Tang et al. 2017; Bagherpour et al., 2017). Even if diagenetic processes can alter  
53 primary geochemical signals (Thomazo et al. 2016), Early Triassic sediments record some of  
54 the largest known Phanerozoic carbon isotope excursions (Atudorei 1999; Payne et al. 2004;  
55 Galfetti et al., 2007; Grasby et al., 2013). Such global and large carbon isotope fluctuations  
56 may reflect severe environmental disturbances – e.g. anoxia, euxinia, hypercapnia, high  
57 temperature, ocean acidification, nutrient-rich waters – that postponed or interfered with the  
58 biotic recovery (Wignall and Twitchett 1996; Payne et al. 2010; Sun et al. 2012; Grice et al.  
59 2005; Knoll et al. 2007; Grasby et al. 2013). Moreover, the amount of skeletal organisms in  
60 the aftermath of the Permian-Triassic extinction was apparently unusually reduced (Baud et  
61 al. 1997; Payne et al. 2006). This managed to an increase in the calcium carbonate saturation  
62 state that could explain the flourishing of microbialites in the Early Triassic (Pruss and Bottjer  
63 2004; Pruss et al. 2006; Bottjer et al. 2008; Ezaki et al. 2008, 2012; Woods 2014;  
64 Abdolmaleki and Tavakoli 2016). However, several authors have argued that some Early  
65 Triassic microbialites developed in normal marine settings rather than in harsh environmental  
66 conditions (Schubert and Bottjer 1992; Olivier et al. 2014, 2016; Collin et al. 2015; Vennin et  
67 al. 2015; Fang et al. 2017). The presence of Early Triassic microbial deposits should also be  
68 analysed by taking into account that a significant number of lineages survived in potential  
69 refugia, and that skeletal organisms can be observed either as intercalated with or included  
70 into microbialites, for instance just after the Permian-Triassic boundary (Brühwiler et al.  
71 2008; Kaim et al. 2010; Hautmann et al. 2011; Forel et al. 2013; Bagherpour et al. 2017; Tang  
72 et al. 2017). Some authors now regard these Early Triassic microbial deposits as part of  
73 diverse, ecologically normal marine ecosystems, qualifying them as “microbialite metazoans”

74 (Yang et al. 2015). Consequently, the debate hinges on whether Early Triassic microbialites  
75 occurred when environmental conditions were hostile to metazoans – notably for CaCO<sub>3</sub>-  
76 precipitating invertebrates (Pörtner et al. 2005), or because the surviving metazoans were too  
77 decimated to rapidly recolonize shallow-marine habitats (Algeo et al. 2011). Therefore,  
78 detailed sedimentological studies are of primary importance for documenting the  
79 palaeoenvironments in which Early Triassic microbial deposits and skeletal metazoans co-  
80 occurred (Kershaw 2017).

81         Along the western margin of Pangea, the Sonoma Foreland Basin of the western USA  
82 was the site of Early Triassic marine sedimentation (Collinson et al. 1976; Paull and Paull  
83 1994; Dickinson 2013; Caravaca et al. 2017). In southwestern Utah, the Lower Triassic  
84 sediments exhibit transitional deposits between the marine Thaynes Group and the continental  
85 Moenkopi Group (*sensu* Lucas et al. 2007a). The Hurricane Cliffs expose various  
86 sedimentary deposits such as conglomerates, sandstones, and microbial and fossiliferous  
87 carbonates (Gregory 1950; Blakey 1979; Lucas et al. 2007a). Several areas give access to  
88 stratal architectures that suggest rapid lateral facies variations over several tens of metres  
89 (Nielson 1991; Olivier et al. 2014). About four kilometres south of the Hurricane airport, near  
90 the head of Workman Wash, exceptional Early Triassic outcrops document the nature and the  
91 spatial relationship between late Smithian microbialites and coeval fossiliferous deposits. The  
92 aim of this paper is (i) to describe the main sedimentary succession at Workman Wash and to  
93 interpret the evolution of the depositional settings, (ii) to demonstrate that microbial and  
94 fossiliferous limestones coexisted as lateral facies belts influenced by relative sea-level  
95 changes, and (iii) to discuss the environmental and ecological significance of such a  
96 microbial-metazoan association in the aftermath of the Permian-Triassic biotic crisis.

97

98

## 99 **2. Geological framework**

100         During the Early Triassic, the western USA was located at a near-equatorial position,  
101 on the western margin of Pangea (Fig. 1b). During the Sonoma Orogeny, the onset of the  
102 Golconda Allochthon led to the formation of a north-south foreland sedimentary basin, which  
103 covered a large area including eastern Nevada, Utah, Idaho and parts of Wyoming (Collinson  
104 et al. 1976; Dickinson, 2006, 2013; Caravaca et al. 2017). From the north towards the south-  
105 southwest, the Sonoma Foreland Basin recorded a major transgressive trend during the  
106 Smithian (Paull and Paull 1993; Goodspeed and Lucas 2007; Brayard et al. 2013). The

107 presence of heterogeneities of the basin basement generated differential flexural subsidence,  
108 which impacted the sedimentary record and thicknesses (Caravaca et al. 2017).

109 The study area is located in Washington County (southwestern Utah, USA), about 8  
110 km south of Hurricane city, near the head of Workman Wash between the Three Brothers and  
111 White Face heights (37°5'56.62''N, 113°17'44.60''W; Fig. 1a). The studied Permian-Triassic  
112 succession is capped by the Three Brothers volcanic rocks, which are remnants of early  
113 Pleistocene lava (<http://geology.utah.gov/apps/intgeomap/index.html>; Hayden, 2004). The  
114 Permian-Triassic transition can be observed on the western side of the Hurricane Cliffs,  
115 whereas only Triassic rocks outcrop on its eastern side along Workman Wash (Fig. 2). Blakey  
116 (1979) was the first to illustrate this area that Brayard et al. (2015) and Jattiot et al. (2017)  
117 later referred to as “Black Rock Canyon”. Lucas et al. (2007a) recently revised the  
118 stratigraphic nomenclature of Early Triassic rocks in southwestern Utah with a lectostratotype  
119 section from Timpoweap Canyon, located a couple of kilometres northeast of Hurricane. For  
120 these authors, Early Triassic rocks of the Hurricane Cliffs begin with a chert breccia unit of  
121 the Rock Canyon Conglomerate Formation (Moenkopi Group), which is overlain by a second  
122 unit comprised of the various types of limestones and calcareous shales of the Sinbad  
123 Formation (Thaynes Group). Finally, limestones of the Sinbad Formation are capped by  
124 clastic deposits of the Lower Red Formation (a new digitation of continental deposits of the  
125 Moenkopi Group; see Figure 2 of Lucas et al. 2007a for subdivisions and lateral correlations  
126 between stratigraphic units of Thaynes and Moenkopi groups). These Triassic deposits rest  
127 unconformably on silicified and recrystallized mudstones of the Permian Kaibab Formation  
128 (Reeside and Bassler 1922; Gregory 1950; Blakey 1979; Stewart et al. 1972; Nielson and  
129 Johnson 1979; Nielson 1991; Olivier et al. 2014). The presence of the ammonoid genera  
130 *Owenites*, *Anasibirites* and *Wasatchites* in the Timpoweap Formation (= junior synonym of  
131 the Sinbad Formation) at Virgin Dam and near Cedar City indicates a middle to late Smithian  
132 age for this stratigraphic unit in this area (Lucas et al. 2007a; Brayard et al. 2013).

133

134

### 135 **3. Studied sections and lithological units**

136 Five sections have been logged between the Three Brothers and the White Face  
137 volcanic peaks (Fig. 1). Section #1 is located on the western side of Hurricane Cliffs (Fig. 2a).  
138 About 300 m away, four additional sections (#2-5) have been logged along the northern flank  
139 of Workman Wash (Fig. 2b). Among them, section #1 provides the most complete  
140 sedimentary succession of Early Triassic deposits that cap Permian limestones of the Kaibab

141 Formation (Figs. 3 and 4). These latter deposits correspond to a succession of dolostones,  
142 dolosiltstones and bioclastic limestones that are more or less dolomitized, silicified and  
143 bioturbated. This Permian succession is interrupted by a pluri-metre thick channelized breccia  
144 interval. Just below this conglomeratic interval, Permian limestones reveal an extensive  
145 karstification extending up to 2 metres thick in this area. A second karstified interval is  
146 observed approximately 3 metres below a surface that probably represents the top of the  
147 Kaibab Formation and the Permian-Triassic transition (Fig. 4). Above this surface, the Early  
148 Triassic sedimentary succession is approximately 70 metres thick. Unfortunately, scree slopes  
149 hide the outcrop 30 metres before the Early Pleistocene basalts that cap the section (Fig. 2b).  
150 This Early Triassic succession displays in ascending order deposits of the Rock Canyon  
151 Conglomerate, Sinbad, and Lower Red formations. Along section #1, deposits of the Rock  
152 Canyon Conglomerate Formation are about 17 metres thick (Fig. 4). They can be subdivided  
153 into 4 successive lithological units. The first one corresponds to a first yellow clastic unit that  
154 is at least 3.5 metres thick. It is overlain by a 3 metres thick red bed unit that is itself capped  
155 by a second yellow clastic unit. A 5 metre thick conglomeratic breccia unit marks the end of  
156 the Rock Canyon Conglomerate Formation. Above it, the Sinbad Formation consists of a  
157 single 18 metre thick fenestral-microbial limestone unit. A third level of yellow clastic  
158 deposits characterizes the uppermost part of the section, which is considered here to belong to  
159 the Lower Red Formation. Section #2 is only 5 metres thick and can be subdivided into two  
160 lithological units of the Sinbad Formation (Fig. 5). Most of this section corresponds to a first  
161 fenestral-microbial unit. The second lithological unit made of bioclastic limestones is only  
162 visible in the first decimetres of the section. Section #3 is around 19 metres thick and can be  
163 subdivided into 4 lithological units (Fig. 6). A basal bioclastic unit, capped by a 12 metre  
164 thick fenestral-microbial unit and a single bed of a pel-fenestral unit represent the deposits of  
165 the Sinbad Formation. The uppermost part of the section corresponds to the yellow limestone  
166 unit of the Lower Red Formation. Section #4 is 16 metres thick and consists of four  
167 lithological units (Fig. 7). A basal breccia unit outcrops over a thickness of one metre; it is  
168 capped by a 4 metre thick fenestral-microbial unit. Above this rests a third bioclastic  
169 lithological unit of more than 7 metres thick. These first three units belong to the Sinbad  
170 Formation. The uppermost part of the section corresponds to the yellow clastic unit of the  
171 Lower Red Formation. Section #5 corresponds to one single, 15 metre thick fenestral-  
172 microbial unit of the Sinbad Formation (Fig. 8).

173

174

## 175 **4. Facies descriptions**

176 A bed-by-bed macro- and microscopic sedimentological analysis of the five sections,  
177 which included the observation of more than 150 thin sections, allowed us to identify 13 main  
178 facies (Table 1). These facies can be grouped into several categories, including terrigenous  
179 (F1, F2), dolomitized (F3-F6), fenestral-microbial limestones (F7) and fossiliferous (F8-F13)  
180 deposits. The fenestral-microbial limestones (F7) appear as the most complex facies in  
181 composition and the most common at the scale of the outcrop.

182

### 183 **4.1. Fenestral-microbial limestones (Facies F7)**

184 Limestones with microbial laminations and fenestrae occur in the five studied sections  
185 (Fig. 9A). Macroscopically, the fenestral-microbial beds sometimes appear truncated, and  
186 more commonly display lateral thickness variations, forming dm-scale lens-like to flat  
187 morphologies (Fig. 10). These fenestral-microbial beds can also locally interfinger with  
188 breccia (F1) or bioclastic (F10) deposits (e.g. section #5 in Fig. 8). Another feature of this  
189 fenestral-microbial facies is to record common lenses of macroscopic skeletal organisms such  
190 as gastropods and ammonoids (Figs. 9C-D and 10). Brayard et al. (2015) identified three main  
191 taxa of gastropods in these levels, corresponding to “*Coelostylina* sp. A”, *Angularia* sp., and  
192 *Worthenia windowblindensis*. All these taxa are large-sized gastropods, with shell sizes  
193 reaching ~ 10 cm in length for the largest sampled specimens of “*Coelostylina* sp. A”.  
194 Sampled ammonoids correspond to a rich and well-preserved prionitid fauna, typical of the  
195 late Smithian *Anasibirites multiformis* beds in the western USA Basin (Brayard et al. 2013;  
196 Jattiot et al. 2016, 2017), including *Anasibirites kingianus*, *A. multiformis*, *Wasatchites*  
197 *perrini*, *Hemiprionites walcotti*, *H. typus* and *Arctoprionites resseri*.

198 Microscopically, F7 is relatively diverse in composition and texture, making it  
199 possible to distinguish 5 subfacies (F7a-e; Table 1). In some cases, fenestral-microbial  
200 deposits are made of abundant pisoids (subfacies F7a; Fig. 11A) or intraclasts (subfacies F7e;  
201 Fig. 11B). Subfacies F7b is characterized by large cm- to dm-scale fenestrae (Fig. 9B).  
202 Diversified endostromatolites, commonly made of irregular to domal micritic laminae or  
203 sparitic laminae (Fig. 11C-E), developed in the fenestrae. Acicular to botryoidal cements are  
204 also observed associated with these endostromatolites (Fig. 11F). Subfacies F7c is  
205 characterized by lamellar siliceous sponges co-occurring with micritic stromatolites and  
206 common ostracods (Fig. 11G and H). Locally, this subfacies records some root-like structures  
207 and circum-granular cracks (Fig. 12A). Subfacies F7d corresponds to microbial-fenestral  
208 deposits that display a conglomeratic nature, with abundant polygenic and subangular to

209 subrounded lithoclasts (Fig. 12B). A common feature shared by all these subfacies includes  
210 the presence of frequent biofilms that are a few tens of microns thick and that have a micritic  
211 nature. These biofilms are observed coating different types of substrates, such as pel-oncoid-  
212 fenestral deposits, pel-ooidal grainstones, or gastropods and ammonoids (Fig. 12C-E). In  
213 other cases, the biofilms developed micritic stromatolites with microscopic planar, irregular to  
214 domal morphologies (Fig. 12F and G). Locally, some cement crusts show enigmatic  
215 structures (Fig. 12H).

216

#### 217 **4.2. Fossiliferous limestones (Facies F8-F13)**

218 Six facies (F8-F13) with a moderately diversified fauna (including echinoderms,  
219 gastropods, siliceous sponges, ostracods, bivalves, lingulid brachiopods, and phosphatic  
220 remains) and a more or less intense degree of bioturbation are identified (Table 1). These  
221 facies are distinguished according to their textures, sedimentary structures, as well as their  
222 grain abundances. Facies F8 is a mud-supported limestone with frequent echinoderms. Facies  
223 F9 is an intensively bioturbated packstone (locally wackestone) with abundant echinoderms  
224 and frequent siliceous sponge spicules (Fig. 13A). Facies F10 is a bioturbated grain-supported  
225 bioclastic (mainly gastropods and bivalves) limestone that also includes abundant ooids (Fig.  
226 13B).

227 Facies F11 corresponds to an intensively bioturbated and bioclastic packstone  
228 composed of abundant bioclasts of gastropods, echinoderms, bivalves and vertebrate  
229 phosphate remains. Beds attributed to this facies displays a spectacular abundance of well-  
230 preserved lingulid brachiopods frequently preserved in their burrows (Figs. 9E and 14). Such  
231 a remarkable macroscopic assemblage deserves a short description here as it has important  
232 implications in terms of depositional setting and palaeoecology. A majority of lingulid  
233 specimens are complete articulated shells preserved perpendicular to the bedding, with the  
234 ventral side upward, showing that they are preserved *in situ* and in life position. The shells are  
235 elongated, twice as long as wide. Most measurable specimens are between 15 and 20 mm in  
236 length; a few complete specimens reach 21 mm. The dorso-ventral thickness is about 5 mm.  
237 The posterior part of the shell is rounded, the anterior part is spade-shaped and the lateral  
238 borders are parallel. Although no internal structure could be observed, these shells are  
239 tentatively attributed to *Lingularia* sp., the most frequent Mesozoic lingulid genus (Biernat  
240 and Emig 1993; Zonneveld et al. 2007; Posenato et al. 2014; Holmer et al. 2016).  
241 Interestingly, the shell length of the specimens found at Workman Wash tends to exceed the  
242 values reported for other Early Triassic lingulids (e.g. Zonneveld et al. 2007, Posenato et al.

243 2014, Peng et al. 2007). Several shells described here are concordantly emplaced in their  
244 dwelling burrows that tend to be deep (about 150 mm), densely distributed locally (about 500  
245 burrows/m<sup>2</sup>) and filled by a yellow-to-orange dolomitized micrite (Fig. 9E). Burrows are  
246 cylindrical, vertical though not totally straight, and rounded to slightly elliptical in cross  
247 section. Many of them correspond to pedicle traces whose diameters are particularly  
248 homogeneous (5 mm in average). Several burrows are spreitenate and they preserve concave-  
249 up laminae whose width is comprised between 8 and 12 mm (Fig. 14B). Some of these  
250 laminae are found immediately below the posterior part of *Lingularia* shells preserved *in situ*  
251 and that have the same width. All these features warrant the identification of these trace  
252 fossils as *Lingulichnus verticalis* that are typical lingulid equilibration traces (Hakes 1976;  
253 Szmuc et al. 1977; Zonneveld and Pemberton 2003; Zonneveld et al. 2007). They are  
254 associated with some U-shaped and J-shaped burrows that we identify as *Lingulichnus*  
255 *hamatus*, an ichnofossils interpreted as a lingulid reburrowing structure (Zonneveld and  
256 Pemberton 2003; Zonneveld et al. 2007). Some horizontal, more or less sinuous traces also  
257 occur on the top of the beds representing facies F11. The dominance of vertical, cylindrical  
258 and U-shaped burrows of suspension feeders, the frequent occurrence of equilibrichnia-  
259 related laminae, the relative rarity of horizontal structures and the low ichnological diversity  
260 suggest an attribution of these beds to the *Skolithos* ichnofacies (Seilacher 1963; Frey and  
261 Seilacher 1980; Frey and Pemberton 1984, 1985; MacEachern et al. 2007; Buatois and  
262 Mángano 2011). Finally, it should be noted that the beds attributed to Facies F11 also yields  
263 large shells of indeterminate bivalves.

264 Facies F12 is a bioclastic packstone-grainstone rich in peloids (Fig. 13C). Facies F13  
265 is a grainstone (locally packstone) notably characterized by frequent intraclasts (Fig. 13D).  
266 Apart from Facies F8 and F9, these bioclastic limestones display dm- to m-scale trough cross  
267 bedding with low angle fore sets or small asymmetrical ripples, and common mud drapes for  
268 F10.

269

#### 270 **4.3. Terrigenous (F1-F2) and other carbonate facies (F3-F6)**

271 In addition to the fenestral-microbial (F7) and bioclastic limestones (F8-F13), 6 other  
272 facies can be identified (Table 1). Facies F1 corresponds to a channelized conglomerate  
273 breccia with angular to subrounded polygenic clasts (Fig. 9F). Facies F2 is a thin-bedded  
274 dolosiltstone with common bioturbation, trough cross stratifications and asymmetrical ripples  
275 that locally display some mud drapes. The remaining facies are carbonate-dominated, but  
276 terrigenous components can be sometimes observed. F3 corresponds to a dolomudstone

277 characterized by some bioturbation and no preserved fauna. F4 is a dolostone devoid of fauna  
278 and sedimentary structures. F5 is a silty peloidal packstone with some bivalves, rare  
279 gastropods and some micritized ooids. This facies is characterized by some mud clasts, mud  
280 drapes and trough cross bedding with low angle foresets. F6 is a wackestone/packstone  
281 limestone with keystone vugs. It is characterized by frequent reworked clasts of microbial  
282 crusts and rare bioturbation.

283  
284

## 285 **5. Multi-scale lateral facies variations**

286 Figure 15 shows the correlation of the 5 studied sections, along which no evidence of  
287 faults was found. Such a correlative scheme is possible because some beds can be laterally  
288 traced across the sections. First, a 20-30 cm thick bed, particularly rich in lingulid  
289 brachiopods in section 4, can be traced laterally through sections #3 and #2. This “lingulid”  
290 marker bed was not found in section #1 and could not be followed laterally into section #5  
291 because of ground vegetation (Fig. 2B). Second, the correlation of section #1 is attempted  
292 through its conglomerate unit that has a lateral equivalent observed at the base of section #4.  
293 Last, the position of section #5 was estimated with a tolerance of few centimetres, in laterally  
294 following as far as possible successive beds of sections #4 and #5.

295 At a first order, the stratigraphic succession of the Black Rock Conglomerate, Sinbad  
296 and Lower Red formations can be easily observed laterally although some lithological units  
297 display important thickness variations. For example, the yellow clastic unit 3 of section #4  
298 stratigraphically starts much lower compared to other sections (Fig. 15). This could be  
299 explained in two ways. First, the yellow clastic unit 3 could lay unconformably over the  
300 fenestral microbial unit, thus explaining changes in thickness between the different sections.  
301 Second, there could be a lateral facies variation between the fenestral microbial unit and this  
302 yellow clastic unit. No evidence of a significant erosional surface has been identified in the  
303 field. Thus, the studied locality likely records lateral facies variations at the scale of few  
304 hundreds of metres. Such lateral facies variations are well expressed in the stratigraphic  
305 distribution of the bioclastic unit. Between sections #3 and #4, the bioclastic facies F12 is  
306 observed laterally to different subfacies of the fenestral-microbial limestone (F7) over a few  
307 tens of metres. Located more than 100 m away, section #5 also records a thin bed of bioclastic  
308 limestone (F10), highlighting again the lateral proximity between fossiliferous and microbial  
309 deposits. In section #5, the intercalation of a dm-scale thick bed of breccia also emphasizes  
310 that such terrigenous sediments are recurrent, even above the Rock Canyon Conglomerate

311 Formation. These observations demonstrate important lateral facies changes over a few tens  
312 of metres in the Hurricane Cliffs area, whereas previous studies only presumed their existence  
313 after larger-scale lithostratigraphic correlations (Blakey 1979; Nielson and Johnson 1979).

314 Some facies changes can also be laterally traced at the scale of a single bed. For  
315 example, across sections #2, #3 and #4, the “lingulid” marker bed exhibits at least two facies.  
316 Over a few tens of metres (Fig. 15), this marker bed is made of a packstone rich in siliceous  
317 sponge spicules (F9), which evolves into an intensively bioturbated limestone with some  
318 lingulids, echinoderms, bivalves and gastropods (F11). As indicated by the number of  
319 identified subfacies, the fenestral-microbial limestone (F7) is probably the facies displaying  
320 the most important changes in terms of composition. Even within a subfacies, the distribution  
321 of some structures such as biofilms or stromatolites has a restricted lateral extension.  
322 Likewise, the presence and abundance of some coated grains such as ooids, oncoids, or  
323 pisoids can shift markedly at the scale of a thin section, not to mention some macroscopic  
324 organisms (ammonoids, gastropods, or ostracods) whose distribution is highly heterogeneous  
325 in this fenestral-microbial limestone. Indeed, some accumulations of gastropods are observed  
326 only in some local dm-scale lenses (Fig. 9C). Similarly, ammonoids also accumulated in  
327 some (pluri)dm-scale lenses (Fig. 9D). Additionally, ammonoids are preferentially  
328 concentrated in some specific beds and over a few tens of decimetres (Fig. 10). On a smaller  
329 scale, some microscopic skeletal organisms such as ostracods also display a similar  
330 heterogeneous distribution. In these fenestral-microbial limestones, ostracods are usually  
331 observed associated with siliceous sponges and stromatolites within sediments displaying a  
332 micritic fabric (Fig. 11G).

333

334

## 335 **6. Depositional environments and relative sea-level fluctuations**

336 Observed sedimentary features point towards a mixed siliciclastic-carbonate marine  
337 depositional system (Fig. 16), whose minimum depth is probably localized within an area  
338 corresponding to a supratidal-subtidal interior platform showing the deposition of fenestral-  
339 microbial limestones (F7). This facies locally records multiple phases of emersions, as  
340 emphasized by frequent pisoids, mud cracks, root structures and truncation surfaces (Figs. 10,  
341 11A, 12A). This fenestral-microbial facies belt thus likely separated an inner tidal flat from a  
342 subtidal interior platform. In the inner tidal flat, terrigenous deposits (F2) dominated the  
343 sedimentation, whereas carbonates only occurred as isolated muddy pools (F3). Additionally,  
344 the correlation scheme suggests that the fenestral-microbial facies belt was not laterally

345 continuous (Fig. 15), but was intersected by broad channels into which fossiliferous  
346 limestones were deposited (F13). Facies F13 includes sedimentary grains (intraclasts) derived  
347 from the fenestral-microbial limestones and bioclasts (echinoderms) characteristic of more  
348 open marine settings. These latter settings correspond to the subtidal interior platform where  
349 various fossiliferous limestones (F8-F12) were deposited. Both in the inner tidal flat and in  
350 the subtidal interior platform, the presence of megaripples with mud drapes and mud clasts  
351 emphasizes a tide-influenced regime. Some fossiliferous limestones (F8 and F9) appear  
352 devoid of tide- or wave-generated sedimentary structures, suggesting the presence of some  
353 protected areas. The presence of breccia (F1), notably intercalated within the fenestral-  
354 microbial limestones, indicates the proximity of the paleoshoreline, echoing previous  
355 observations by Olivier et al. (2014) in the vicinity of Workman Wash. This facies (F1)  
356 displays poorly sorted and angular clasts of cherts and limestones that suggest debris flows  
357 derived from the Permian Kaibab Formation. Such facies models also fit well with previous  
358 paleoenvironmental reconstructions, which highlighted a sedimentary system characterized by  
359 a clear polarity with an open sea that stood east of the Hurricane Cliffs (Blakey, 1979). The  
360 relatively small size of the Workman Wash depositional system, also characterized by a flat  
361 slope and a tidal autocyclic character, generated the rapid facies displacements and the  
362 important lateral facies variations observed at the scale of a few tens to hundreds of metres  
363 (Fig. 15).

364 The studied Early Triassic stratigraphic column, which involves three successive  
365 formations (Rock Canyon Conglomerate, Sinbad, Lower Red), displays a clear evolution of  
366 the type of sediments and thus of depositional settings (Figs. 15 and 16). The transition from  
367 proximal and shallow deposits (F2-F4) of the siliciclastic units (Rock Canyon Conglomerate  
368 Formation) to the carbonates (F7) of the fenestral-microbial unit (Sinbad Formation) is  
369 consistent with an increase in accommodation coupled with the general retrogradation of  
370 these facies belts. The high accumulation of fenestral-microbial limestones (F7) explains the  
371 frequent traces of emersion recorded by this facies, despite a more distal and deeper position  
372 in the interior platform. The installation of bioclastic and bioturbated facies in the *Anasibirites*  
373 *multiformis* beds (Brayard et al. 2013; Jattiot et al. 2017) likely reflects a maximum of  
374 accommodation recorded in the Workman Wash area. The return of inner tidal flat siliciclastic  
375 deposits (F5) in the yellow clastic unit 3 (Lower Red Formation) probably marked an  
376 accommodation decrease and a rapid facies progradation. Such facies evolution fits well with  
377 the Smithian third order transgressive-regressive sequence recorded in the western USA

378 Lower Triassic succession (Paull and Paull 1993, 1997), which is characterized by an early-  
379 middle Smithian transgression (Goodspeed and Lucas 2007; Brayard et al. 2013).

380

381

## 382 **7. Ecological and environmental implications**

383 It is usually assumed that a return to pre-extinction levels of taxonomic and functional  
384 diversity after the end-Permian extinction crisis did not occur until the end of the Early  
385 Triassic, or at least late in the Spathian (Schubert and Bottjer, 1995; Flügel 2002; Payne et al.  
386 2006; Lehrmann et al. 2006; Chen and Benton 2012; Pietsch and Bottjer 2014; but see e.g.  
387 Brayard et al. 2009, 2017; Foster et al. 2015). In the presumed absence of developed benthic  
388 faunas, Early Triassic microbialites have been initially considered as disaster forms (i.e.  
389 opportunistic generalist taxa *sensu* Schubert and Bottjer 1992). These disaster microbialites  
390 were first considered to have formed in normal marine settings (Schubert and Bottjer 1992,  
391 1995), like several subsequent studies (Kershaw et al. 1999; Lehrmann 1999; Lehrmann et al.  
392 2001; Ezaki et al. 2008; Yang et al. 2011). Nevertheless, as noted by Tang et al. (2017), Early  
393 Triassic microbialites were progressively reinterpreted to have flourished as a consequence of  
394 harsh environmental conditions, such as hot temperatures, high carbonate saturation, or  
395 elevated CO<sub>2</sub> (Pruss and Bottjer 2004; Pruss et al. 2006; Mary and Woods 2008; Mata and  
396 Bottjer 2011; Pietsch et al. 2014; Song et al. 2014; Abdolmaleki and Tarakoli 2016).  
397 Lehrmann et al. (2015) suggested that ecological relaxation and abnormal ocean chemistry  
398 were not mutually exclusive to explain the proliferation of Early Triassic microbial deposits.  
399 However, diversified assemblages have been documented from various Early Triassic  
400 intervals and latitudes (Krystyn et al. 2003; Twitchett et al. 2004; Beatty et al. 2008; Kaim et  
401 al. 2010; Hautmann et al. 2011, 2013; Hofmann et al. 2011, 2013a, b, 2014; Baud et al. 2015;  
402 Fu et al. 2016; Foster et al. 2017; Brosse et al. in press). Moreover, the onset of complex  
403 ecosystems is now documented to have occurred rapidly after the end-Permian mass  
404 extinction (Haig et al. 2015; Brayard et al. 2017). Hence, the scenario of an ecological  
405 vacation that led to a global post-extinction delayed recovery has become increasingly  
406 unlikely. Moreover, new evidences that Early Triassic microbialites could have formed in  
407 normal marine environments are growing (Olivier et al. 2014, 2016; Vennin et al. 2015; Tang  
408 et al. 2017; Bagherpour et al. 2017). Therefore, the causes of the Early Triassic microbialite  
409 proliferation and their relationships with a delayed biotic recovery scenario remain highly  
410 controversial. This notably results from the poor knowledge of the physico-chemical  
411 parameters of Early Triassic seas into which microbialite developed. Indeed, such

412 palaeoenvironments are reconstructed from analyses of the microbialites themselves without  
413 information from lateral coeval sediments. Sedimentological and palaeontological data from  
414 other types of coeval sediments can indeed indirectly provide insights on the chemical  
415 composition of waters in which microbial deposits developed (Bagherpour et al. 2017).

416

417         Among the four episodes of microbialite expansion initially identified for the Early  
418 Triassic (Pruss et al. 2006; Baud et al. 2007), only the Permian-Triassic boundary  
419 microbialites (PTBMs) have a geographical extent large enough to have a global significance  
420 (Kershaw et al. 2012). Deep-water forms of PTBMs with metazoans are known and recently  
421 described by Baud et al. (2017) and by Friesenbichler et al. (2018). Within interior platform  
422 PTBMs, skeletal remains of some brachiopods, bivalves, microconchids, gastropods,  
423 echinoderms and sparse ammonoids are mainly observed as interstratified beds or lenses  
424 (Lehrmann et al. 2001; Baud 2007; Hautmann et al. 2015; Tang et al. 2017; Bagherpour et al.  
425 2017). Thus, reliable ecological and environmental information from contemporaneous  
426 deposits of PTBMs remains to be documented in more detail.

427         Post-PTBMs microbial episodes in the Early Triassic have much more restricted  
428 geographic distributions (Mata and Bottjer 2012). Those observed in the southwestern USA  
429 basin are crucial since local and regional studies suggest the existence of lateral correlations  
430 between Smithian microbialites and different types of sediments containing an abundant and  
431 diversified fauna (i.e. brachiopods, bivalves, gastropods, ostracods, echinoderms, sponges and  
432 ammonoids; Stewart et al. 1972; Blakey 1974, 1977; Nielson and Johnson 1979; Dean 1981;  
433 Nielson 1991; Goodspeed and Lucas 2007; Ritter et al. 2013; Olivier et al. 2016). However, a  
434 major challenge on the field lies in the capacity to observe and to demonstrate the lateral  
435 transition and the contact between microbial deposits and these open marine skeletal  
436 limestones. Such lateral facies variation has been observed along an outcrop a few tens of  
437 meters long in Timpoweap Canyon, north of the Hurricane Cliffs (Olivier et al. 2014). At this  
438 site, a fenestral-microbial limestone deposited in contact with a dolomudstone characterized  
439 by sparse bioturbations and rare bioclasts (serpulids, bivalves and echinoderms). A few  
440 meters away, this mudstone evolves into a bioturbated limestone with a wackestone (locally  
441 packstone) texture and some gastropods, serpulids, bivalves and echinoderm plates. However,  
442 the limited extent of this outcrop does not provide a good spatial comprehension of its  
443 depositional setting.

444         At Workman Wash, the lateral continuity of deposits over a few hundred meters  
445 highlights the lateral transition between fenestral-microbial deposits and limestones

446 characterized by a relatively abundant metazoan fauna (Figs. 15 and 16). With some ostracods  
447 and gastropods, the fauna observed in the fenestral-microbial facies is neither diversified nor  
448 abundant, reflecting a microbe-dominated ecosystem. As microbialites flourished on this  
449 shallow sea floor of the internal platform, they were potentially a profuse resource for grazing  
450 gastropods (Batten and Stokes 1986; Schubert and Bottjer 1995; Pietsch et al. 2014), although  
451 this hypothesis remains to be corroborated (see discussion in Brayard et al. 2015).  
452 Furthermore, sponges are also observed associated with microbialites (Fig. 11G, H). This  
453 confirms the common occurrence of these metazoan reef-builders in Early Triassic reefs  
454 (Brayard et al. 2011; Marengo et al 2012; Baud 2013, Vennin et al. 2015; Olivier et al. 2016;  
455 Baud et al. 2017; Friesenbichler et al. 2018). It implies that the local trophic network not only  
456 consisted of primary but also meso-consumers such as sponges. The common lenses of  
457 ammonoids preserved in the Workman Wash microbialites indicate the presence of higher-  
458 level consumers. The abundant lingulid brachiopods observed in a 30 cm thick interval could  
459 also be interpreted as opportunist meso-consumers (Rodland and Bottjer 2001). Thus,  
460 considered separately, both the microbial or lingulid-rich facies actually do not illustrate an  
461 ecosystem with a trophic level higher than microbe-dominated and possibly opportunist-  
462 dominated ones (Chen and Benton 2012). However, even if lingulid brachiopods are  
463 effectively common in some beds, the facies F11 in which they occur also includes frequent  
464 to abundant fragments of crinoids, gastropods and bivalves (Fig. 16). These observations  
465 better fit recent studies that point toward lingulids as ecological opportunists that dominated  
466 locally in some Early Triassic shallow marine environments rather than a disaster taxon  
467 (Zonneveld et al. 2007; McGowan et al. 2009). Other adjacent deposits of microbialites such  
468 as the facies F9 also comprises abundant elements of crinoids and frequent sponge spicules,  
469 coupled with an abundant infaunal activity. Overall, the depositional system reconstructed at  
470 Workman Wash shows that microbial and lingulid-dominant deposits are coeval with a  
471 moderately diversified benthic metazoan ecosystem. Such a biocoenosis including siliceous  
472 sponges (either present in reefs or in lateral deposits), crinoids, lingulid brachiopods, large-  
473 size gastropods and higher-level consumers, such as ammonoids and vertebrates, indicates  
474 that some Early Triassic marine ecosystems were not ecologically depauperate (Krystyn et al.  
475 2003; Foster and Twitchett 2014; Baud et al. 2015; Brosse et al. in press). Additionally, the  
476 actual diversity of the Workman Wash palaeocommunity is probably underestimated, as  
477 suggested by ammonoids that are only preserved in the microbial-fenestral facies. Indeed,  
478 microbial deposits are known to favour rapid sediment stabilization and early lithification  
479 (Gall 1990; Tomescu et al. 2016). This may explain a differential preservation of some

480 organisms such as ammonoids. All these mechanisms highlight how differential taphonomic  
481 pathways can bias the fossil record in some Early Triassic marine settings.

482

483 From an environmental point of view, the presence of stenohaline organisms such as  
484 echinoderms in deposits lateral to the microbial-fenestral facies indicates normal marine  
485 conditions. The abundant lingulids observed in facies F11 also reflect an intense infaunal  
486 activity, implying the presence of nutrient-rich waters. The proximity of emerged lands may  
487 have provided an adequate nutrient supply to the depositional system, which in turn could  
488 have promoted the development of microbialites (Algeo et al. 2011; Olivier et al. 2016). In  
489 subtidal settings of the inner tidal flat (Fig. 16), the presence of an important terrigenous flux  
490 and intense sediment mobility (caused by tidal currents) could have inhibited microbialite  
491 development (Olivier et al., 2016). In such siliciclastic peritidal environments, microbial  
492 deposits are nevertheless known in other Early Triassic successions of the Sonoma Foreland  
493 Basin as microbially induced sedimentary structures (MISS; Grosjean et al., 2018). In the  
494 more open subtidal settings of the interior platform, the abundance of lingulid equilibration  
495 structures (in response to burial) and reburrowing structures (in response to exhumation) are  
496 consistent with a tidal regime. This relatively intense infaunal activity, coupled with the  
497 migration of tidal bars, may have prevented the development of microbialites in the more  
498 distal parts of the Workman Wash depositional setting.

499

500

## 501 **8. Conclusions**

502 For the first time, the late Smithian rocks of Workman Wash in the Northern  
503 Hurricane Cliffs (southwestern Utah, USA) provide a direct and continuous observation of the  
504 lateral facies transition between microbialites and contemporaneous fossiliferous limestones  
505 in the Early Triassic. Facies analysis reveals a shallow and proximal tide-dominated and  
506 mixed siliciclastic-carbonate sedimentary system. It was located along the southwestern  
507 margin of an epicontinental sea tongue corresponding to the Sonoma Foreland Basin. Above  
508 Permian limestones, the studied interval includes breccia and dolosiltstones of the Rock  
509 Canyon Conglomerate Formation, fenestral-microbial and bioclastic limestones of the Sinbad  
510 Formation, and yellow dolosiltstones of the Lower Red Formation. This lithological  
511 succession is in accordance with the Smithian third-order transgressive-regressive sequence  
512 recorded in the western USA.

513            Located in an interior platform and over only a few hundreds of meters, intertidal to  
514 subtidal microbialites pass laterally to bioturbated and fossiliferous limestones containing a  
515 moderately abundant and diversified fauna including echinoderms, lingulid brachiopods,  
516 gastropods, bivalves, ostracods, siliceous sponges and vertebrate remains. Such a faunal  
517 assemblage coeval with microbialites reveals a moderately diversified biocoenosis, which is  
518 in stark contrast to traditional views of depauperate ecosystems in the Early Triassic. The  
519 fossiliferous limestones comprising stenohaline organisms also suggest normal marine  
520 conditions contrary to the harsh environmental conditions classically invoked to explain the  
521 presence of microbialites. At Workman Wash, microbialites rather reflect a shallow and  
522 proximal facies belt controlled by terrigenous flux, nutrient inputs and relative sea-level  
523 fluctuations.

524

525

526

527

## 528 **Acknowledgements**

529 This work is a contribution to the ANR project AFTER (ANR-13-JS06-0001-01). The CNRS  
530 INSU Interrvie, and the French ANR @RAction grant (project EvoDevOdonto) also  
531 supported this study. D.A. Stephen is grateful for the ongoing financial support of the College  
532 of Science & Health at Utah Valley University. Michael Hautmann is thanked for his  
533 assistance in bivalve taxonomy and ecology. Our thanks to Marilyne Imbault for her  
534 contribution to the ammonoid determination. The Workman Wash area is located on US  
535 public land under the stewardship of the Bureau of Land Management (BLM) of the US  
536 Department of the Interior; access to this land is gratefully acknowledged. We would like to  
537 thank Wolfgang Kießling and two anonymous reviewers for their helpful comments.

538

539

540

541

## 542 **References**

543 Abdolmaleki J, Tavakoli V (2016) Anachronistic facies in the Early Triassic successions of  
544 the Persian Gulf and its palaeoenvironmental reconstruction. *Palaeogeogr Palaeoclimatol*  
545 *Palaeoecol* 446:213–224

546 Algeo TJ, Chen ZQ, Fraiser ML, Twitchett RJ (2011) Terrestrial–marine teleconnections in  
547 the collapse and rebuilding of Early Triassic marine ecosystems. *Palaeogeogr*  
548 *Palaeoclimatol Palaeoecol* 308:1–11

549 Atudorei NV (1999) Constraints on the Upper Permian to Upper Triassic marine carbon  
550 isotope curve. Case studies from the Tethys. PhD thesis, University of Lausanne:1–155

551 Bagherpour B, Bucher H, Baud A, Brosse M, Vennemann, T, Martini R, Guodun K (2017)  
552 Onset, development, and cessation of basal Early Triassic microbialites (BETM) in the  
553 Nanpanjiang pull-apart Basin, South China Block. *Gondwana Res* 44:178–204

554 Batten RL, Stokes WL (1986) Early Triassic gastropods from the Sinbad Member of the  
555 Moenkopi Formation, San Rafael Swell, Utah. *American Mus Novit* 2864:1–33

556 Baud A (2007) Lower Triassic microbialites versus skeletal carbonates, a competition on the  
557 Gondwana Margin. *N M Mus Nat Hist Sci Bull* 41:23

558 Baud A (2013) The Smithian (Early Triassic) red ammonoid limestone of Oman, refuge for  
559 sponge-microbial build-ups during recovery phase. GSA Annu Meet in Denver

560 Baud A, Cirilli S, Marcoux J (1997) Biotic response to mass extinction: the lowermost  
561 Triassic microbialites. *Facies* 36:238–242

562 Baud A, Richoz S, Pruss S (2007) The lower Triassic anachronistic carbonate facies in space  
563 and time. *Global Planet Change* 55:81–89

564 Baud A, Friesenbichler E, Richoz S, Krystyn L, Sahakyan L, (2017) Induan (Early Triassic)  
565 giant sponge-microbial build-ups in Armenia. 5th IGCP 630 International conference and  
566 field workshop, Erevan 8-14 October 2017 Program and Abstract: 13.

567 Beatty TW, Zonneveld JP, Henderson CM (2008) Anomalously diverse Early Triassic  
568 ichnofossil assemblages in northwest Pangea: A case for a shallow-marine habitable zone.  
569 *Geology* 36(10):771–774

570 Biernat G, Emig CC (1993) Anatomical distinctions of the Mesozoic lingulide brachiopods.  
571 *Acta Palaeontol Pol* 38:1–20

572 Blakey RC (1974) Stratigraphic and depositional analysis of the Moenkopi Formation,  
573 Southeastern Utah. *Utah Geol Miner Surv Bull* 104:1–81

574 Blakey RC (1977) Petroliferous lithosomes in the Moenkopi Formation, Southern Utah. *Utah*  
575 *Geol* 4:67–84

576 Blakey RC (1979) Oil impregnated carbonate rocks of the Timpoweap Member Moenkopi  
577 Formation, Hurricane Cliffs area, Utah and Arizona: *Utah Geol* 6:45–54

578 Bottjer DJ, Clapham ME, Fraiser ML, Powers CM (2008) Understanding mechanisms for the  
579 end-Permian mass extinction and the protracted Early Triassic aftermath and recovery.  
580 *GSA Today* 18:4–10

581 Brayard A, Escarguel G, Bucher H, Monnet C, Brühwiler T, Goudemand N, Galfetti T, Guex  
582 J (2009) Good genes and good luck: Ammonoid diversity and the end-Permian mass  
583 extinction. *Science* 325: 1118-1121

584 Brayard A, Vennin E, Olivier N, Bylund KG, Jenks J, Stephen DA, Bucher H, Hofmann R,  
585 Goudemand N, Escarguel G (2011) Transient metazoan reefs in the aftermath of the end-  
586 Permian mass extinction. *Nature Geosci* 4:693–697

587 Brayard A, Bylund KG, Jenks JF, Stephen DA, Olivier N, Escarguel G, Fara E, Vennin E  
588 (2013) Smithian ammonoid faunas from Utah: implications for Early Triassic  
589 biostratigraphy, correlations and basinal paleogeography. *Swiss J Palaeontol* 132:141–219

590 Brayard A, Meier M, Escarguel G, Fara E, Nützel A, Olivier N, Bylund KG, Jenks JF,  
591 Stephen DA, Hautmann M, Vennin E, Bucher H (2015) Early Triassic Gulliver gastropods:  
592 spatio-temporal distribution and significance for the biotic recovery after the end-Permian  
593 mass extinction. *Earth Sci Rev* 146:31–64

594 Brayard A, Krumenacker LJ, Botting JP, Jenks JF, Bylund KG, Fara E, Vennin E, Olivier N,  
595 Goudemand N, Saucède T, Charbonnier S, Romano C, Doguzhaeva L, Thuy B, Hautmann  
596 M, Stephen DA, Thomazo C, Escarguel G (2017) Unexpected Early Triassic marine  
597 ecosystem and the rise of the Modern evolutionary fauna. *Science Adv* 3:e1602159

598 Brosse M, Bucher H, Baud A, Hagdorn H, Hautmann M, Nützel A, Ware D, Frisk Å,  
599 Goudemand N (in press) New data from Oman indicate benthic high biomass productivity  
600 coupled with low taxonomic diversity in the aftermath of the Permian-Triassic Boundary  
601 mass extinction. *Lethaia*.

602 Brühwiler T, Brayard A, Bucher H, Guodun K (2008) Griesbachian and Dienerian (Early  
603 Triassic) ammonoid faunas from northwestern Guangxi and southern Guizhou (south  
604 China). *Palaeontol* 51:1151–1180

605 Buatois LA, Mángano, MG (2011) *Ichnology: Organism-substrate interactions in space and*  
606 *time*. Cambridge University Press

607 Caravaca G, Brayard A, Vennin E, Guiraud M, Grosjean AS, Olivier N, Thomazo C, Fara E,  
608 Escarguel G, Bylund K, Jenks J (2017) Controlling factors for differential subsidence in  
609 the Sonoma Foreland Basin (Early Triassic, western USA). *Geol Mag* In press.  
610 10.1017/S0016756817000164

- 611 Chen ZQ, Benton, MJ (2012) The timing and pattern of biotic recovery following the end-  
612 Permian mass extinction. *Nature Geosci* 5:375–383
- 613 Collin PY, Kershaw S, Tribovillard N, Forel MB, Crasquin S (2015) Geochemistry of post-  
614 extinction microbialites as a powerful tool to assess the oxygenation of shallow marine  
615 water in the immediate aftermath of the end-Permian mass extinction. *Int J Earth Sci*  
616 104:1025–1037
- 617 Collinson JW, Kendall CGSC, Marcantel JB (1976) Permian–Triassic boundary in eastern  
618 Nevada and west-central Utah. *Bulletin of the Geological Society of America* 87:821–824
- 619 Dean JS (1981) Carbonate petrology and depositional environments of the Sinbad Limestone  
620 Member of the Moenkopi Formation in the Teasdale Dome Area, Wayne and Garfield  
621 Counties, Utah. *Brigham Young Univ Geol Stud* 28:19–51
- 622 Dickinson WR (2006) Geotectonic evolution of the Great Basin. *Geosphere* 2:353–368
- 623 Dickinson WR (2013) Phanerozoic palinspastic reconstructions of Great Basin geotectonics  
624 (Nevada-Utah, USA). *Geosph* 9:1384–1396
- 625 Erwin DH (1996) Understanding biotic recoveries: extinction, survival, and preservation  
626 during the end-Permian mass extinction. *Evolutionary paleobiology*. University of Chicago  
627 Press, Chicago: 398–418
- 628 Erwin DH (2001) Lessons from the past: biotic recoveries from mass extinctions. *Proc Natl*  
629 *Acad Sci USA* 98:5399–5403
- 630 Ezaki Y, Liu J, Nagano T, Adachi N (2008) Geobiological aspects of the earliest Triassic  
631 microbialites along the southern periphery of the tropical Yangtze Platform: initiation and  
632 cessation of a microbial regime. *Palaios* 23:356–369
- 633 Ezaki Y, Liu JB, Adachi N (2012) Lower Triassic stromatolites in Luodian County, Guizhou  
634 Province, South China: evidence for the protracted devastation of the marine  
635 environments. *Geobiol* 10:48–59
- 636 Fang Y, Chen ZQ, Kershaw S, Li Y, Luo M (2017) An Early Triassic (Smithian) stromatolite  
637 associated with giant ooid banks from Lichuan (Hubei Province), South China:  
638 Environment and controls on its formation. *Palaeogeogr Palaeoclimatol Palaeoecol* in press
- 639 Flügel E (2002) Triassic reef patterns. *Phanerozoic Reef Patterns*. *SEPM*: 391–463
- 640 Forel MB, Crasquin S, Kershaw S, Collin PY (2013) In the aftermath of the end-Permian  
641 extinction: the microbialite refuge? *Terra Nova* 25:137–143
- 642 Foster WJ, Twitchett RJ (2014) Functional diversity of marine ecosystems after the Late  
643 Permian mass extinction event. *Nature Geosci* 7:233–238

644 Foster WJ, Danise S, Sedlacek A, Price GD, Hips K, Twitchett RJ (2015) Environmental  
645 controls on the post-Permian recovery of benthic, tropical marine ecosystems in western  
646 Palaeotethys (Aggtelek Karst, Hungary). *Palaeogeogr Palaeoclimatol Palaeoecol* 440:374–  
647 394

648 Foster WJ, Danise S, Price GD, Twitchett RJ (2017) Subsequent biotic crises delayed marine  
649 recovery following the late Permian mass extinction event in northern Italy. *PloS One* 12:  
650 e0172321

651 Frey RW, Seilacher A (1980) Uniformity in marine invertebrate ichnology. *Lethaia* 13:183–  
652 207

653 Frey RW, Pemberton SG (1984) Trace Fossil Facies Models. In: Walker RG (ed) *Facies*  
654 *Models*, 2nd edn. Geosci Canada, Reprint Series 1(41), pp 223–237

655 Frey RW, & Pemberton, S. G. (1985). Biogenic structures in outcrops and cores. I.  
656 Approaches to ichnology. *Bull Can Pet Geol* 33:72–115

657 Friesenbichler E, Richo S, Baud A, Krystyn L, Sahakyan L, Vardanyan S, Peckmann J,  
658 Reitner J, Heindel K (2018) Sponge-microbial build-ups from the lowermost Triassic  
659 Chanakhchi section in southern Armenia: Microfacies and stable carbon isotopes.  
660 *Palaeogeogr Palaeoclimatol Palaeoecol* 90:653–672

661 Fu W, Jiang DY, Montañez IP, Meyers SR, Motani R, Tintori A (2016) Eccentricity and  
662 obliquity paced carbon cycling in the Early Triassic and implications for post-extinction  
663 ecosystem recovery. *Sci rep* 6:27793

664 Galfetti T, Bucher H, Ovtcharova M, Schaltegger U, Brayard A, Brühwiler T, Goudemand N,  
665 Weissert H, Hochuli PA, Cordey F, Guodun K (2007) Timing of the Early Triassic carbon  
666 cycle perturbations inferred from new U–Pb ages and ammonoid biochronozones. *Earth*  
667 *Planet Sci Lett* 258:593–604

668 Gall JC (1990) Les voiles microbiens. Leur contribution a la fossilisation des organismes au  
669 corps mou. *Lethaia* 23:21–28

670 Goodspeed TH, Lucas SG (2007) Stratigraphy, sedimentology, and sequence stratigraphy of  
671 the Lower Triassic Sinbad Formation, San Rafael Swell, Utah. *N M Mus Nat Hist Sci Bull*  
672 40:91–101

673 Grasby SE, Beauchamp B, Embry A, Sanei H (2013) Recurrent Early Triassic ocean anoxia.  
674 *Geology* 4:175–178

675 Gregory HE (1950) Geology and geography of the Zion [National] Park region, Utah and  
676 Arizona. *U S Geol Surv Prof Pap* 220:1–200

677 Grice K, Cao C, Love GD, Böttcher ME, Twitchett RJ, Grosjean E, Summons RE, Turgeon  
678 SC, Dunning W, Jin Y (2005) Photic zone euxinia during the Permian-Triassic  
679 superanoxic event. *Science* 307:706–709

680 Grosjean AS, Vennin E, Olivier N, Caravaca G, Thomazo C, Fara E, Escarguel G, Bylund  
681 KG, Jenks JF, Stephen DA, Brayard A (2018) Early Triassic environmental dynamics and  
682 microbial development during the Smithian–Spathian transition (Lower Weber Canyon,  
683 Utah, USA). *Sediment Geol* 363:136–151

684 Haig DW, Martin SK, Mory AJ, McLoughlin S, Backhouse J, Berrell RW, Kear BP, Hall R,  
685 Foster CB, Shi GR, Bevan JC (2015) Early Triassic (early Olenekian) life in the interior of  
686 East Gondwana: mixed marine–terrestrial biota from the Kockatea Shale, Western  
687 Australia. *Palaeogeogr Palaeoclimatol Palaeoecol* 417:511–533

688 Hakes WG (1976) Trace fossils and depositional environment of four clastic units, Upper  
689 Pennsylvanian megacyclothems, northeast Kansas. *Univ Kans Paleontol Contrib Artic*  
690 63:46 p

691 Hautmann M, Bucher H, Brühwiler T, Goudemand N, Kaim A, Nützel A (2011) An  
692 unusually diverse mollusc fauna from the earliest Triassic of South China and its  
693 implications for benthic recovery after the end-Permian biotic crisis. *Geobios* 44:71–85

694 Hautmann M, Smith AB, McGowan AJ, Bucher H (2013) Bivalves from the Olenekian (Early  
695 Triassic) of south-western Utah: systematics and evolutionary significance. *J Syst*  
696 *Palaeontol* 11:263–293

697 Hautmann M, Bagherpour B, Brosse M, Frisk Å, Hofmann R, Baud A, Nützel A, Goudemand  
698 N, Bucher H (2015) Competition in slow motion: the unusual case of benthic marine  
699 communities in the wake of the end-Permian mass extinction. *Palaeontol* 58:871–901

700 Hayden JM (2004) Geologic map of The Divide quadrangle, Washington County, Utah, Utah  
701 Geological Survey Map 197, scale 1:24,000: 32 p

702 Hofmann R, Goudemand N, Wasmer M, Bucher H, Hautmann M (2011) New trace fossil  
703 evidence for an early recovery signal in the aftermath of the end-Permian mass extinction.  
704 *Palaeogeogr Palaeoclimatol Palaeoecol* 310:216–226

705 Hofmann R, Hautmann M, Bucher, H (2013a) A new paleoecological look at the Dinwoody  
706 Formation (Lower Triassic, western USA): intrinsic versus extrinsic controls on ecosystem  
707 recovery after the end-Permian mass extinction. *J Paleontol* 87:854–880

708 Hofmann R, Hautmann M, Wasmer M, Bucher H (2013b) Palaeoecology of the Spathian  
709 Virgin Formation (Utah, USA) and its implications for the Early Triassic recovery. *Acta*  
710 *Palaeontol Pol* 58:149–173

711 Hofmann R, Hautmann M, Brayard A, Nützel A, Bylund KG, Jenks JF, Vennin E, Olivier N,  
712 Bucher H (2014) Recovery of benthic marine communities from the end-Permian mass  
713 extinction at the low latitudes of eastern Panthalassa. *Palaeontol* 57:547–589

714 Holmer LE, Popov LE, Klishevich I, Ghobadi Pour M (2016) Reassessment of the early  
715 Triassic lingulid brachiopod '*Lingula borealis*' Bittner, 1899 and related problems of  
716 lingulid taxonomy. *GFF*, doi:10.1080/11035897.2016.1149216

717 Jattiot R, Bucher H, Brayard A, Monnet C, Jenks JF, Hautmann M (2016) Revision of the  
718 genus *Anasibirites* Mojsisovics (Ammonoidea): an iconic and cosmopolitan taxon of the  
719 late Smithian (Early Triassic) extinction. *Pap Palaeontol* 2:155–188

720 Jattiot R, Bucher H, Brayard A, Brosse M, Jenks J, Bylund KG (2017) Smithian ammonoid  
721 faunas from northeastern Nevada: implications for Early Triassic biostratigraphy and  
722 correlation within the western USA basin. *Palaeontogr Abt A* 309: 1–89

723 Kaim A, Nützel A, Bucher H, Brühwiler T, Goudemand N (2010) Early Triassic (Late  
724 Griesbachian) gastropods from South China (Shanggan, Guangxi). *Swiss J Geosci*  
725 103:121–128

726 Kershaw S (2017) Palaeogeographic variation in the Permian–Triassic boundary  
727 microbialites: A discussion of microbial and ocean processes after the end-Permian mass  
728 extinction. *J Palaeogeogr* 6:97–107

729 Kershaw S, Zhang T, Lan G (1999) A ?microbialite carbonate crust at the Permian–Triassic  
730 boundary in South China, and its palaeoenvironmental significance. *Palaeogeogr*  
731 *Palaeoclimatol Palaeoecol* 146:1–18

732 Kershaw S, Crasquin S, Li Y, Collin PY, Forel MB, Mu X, Baud A, Wang Y, Xie S, Maurer  
733 F, Guo L (2012) Microbialites and global environmental change across the Permian–  
734 Triassic boundary: a synthesis. *Geobiol* 10:25–47

735 Knoll AH, Bambach RK, Payne JL, Pruss S, Fischer WW (2007) Paleophysiology and end-  
736 Permian mass extinction. *Earth Planet Sci Lett* 256:295–313

737 Lehrmann DJ (1999) Early Triassic calcimicrobial mounds and biostromes of the  
738 Nanpanjiang basin, south China. *Geology* 27:359–362

739 Lehrmann DJ, Wan Y, Wei J, Yu Y, Xiao J (2001) Lower Triassic peritidal cyclic limestone:  
740 an example of anachronistic carbonate facies from the Great Bank of Guizhou,  
741 Nanpanjiang Basin, Guizhou province, South China. *Palaeogeogr Palaeoclimatol*  
742 *Palaeoecol* 173:103–123

743 Lehrmann DJ, Ramezani J, Bowring SA, Martin MW, Montgomery P, Enos P, Payne JL,  
744 Orchard MJ, Wang H, Wei J (2006) Timing of recovery from the end-Permian extinction:  
745 Geochronologic and biostratigraphic constraints from south China. *Geology* 34:1053–1056  
746 Lehrmann DJ, Bentz JM, Wood T, Goers A, Dhillon R, Akin S, Li X, Payne JL, Kelley BM,  
747 Meyer KM, Schaal EK, Suarez MB, Yu M, Qin Y, Li R, Minzoni M, Henderson CM  
748 (2015) Environmental controls on the genesis of marine microbialites and dissolution  
749 surface associated with the end-Permian mass extinction: new sections and observations  
750 from the Nanpanjiang Basin, South China. *Palaios* 30:529–552  
751 Lucas SG, Krainer K, Milner AR (2007a) The type section and age of the Timpoweap  
752 Member and stratigraphic nomenclature of the Triassic Moenkopi Group in Southwestern  
753 Utah. *N M Mus Nat Hist Sci Bull* 40:109–117  
754 Lucas SG, Goodspeed TH, Estep JW (2007b) Ammonoid biostratigraphy of the Lower  
755 Triassic Sinbad Formation, East-Central Utah. *N M Mus Nat Hist Sci Bull* 40:103–108  
756 MacEachern JA, Pemberton SG, Gingras MK, Bann KL (2007) *The Ichnofacies Paradigm-*  
757 *Chapter 4: A Fifty-Year Retrospective*  
758 Marengo PJ, Griffin JM, Fraiser ML, Clapham M E (2012) Paleoecology and geochemistry of  
759 Early Triassic (Spathian) microbial mounds and implications for anoxia following the end-  
760 Permian mass extinction. *Geology* 40:715–718  
761 Mary M, Woods AD (2008) Stromatolites of the Lower Triassic Union Wash Formation, CA:  
762 evidence for continued post-extinction environmental stress in western North America  
763 through the Spathian. *Palaeogeogr Palaeoclimatol Palaeoecol* 261:78–86  
764 Mata SA, Bottjer DJ (2011) Origin of Lower Triassic microbialites in mixed carbonate-  
765 siliciclastic successions: ichnology, applied stratigraphy, and the end-Permian mass  
766 extinction. *Palaeogeogr Palaeoclimatol Palaeoecol* 300:158–178  
767 Mata SA, Bottjer DJ (2012) Microbes and mass extinctions: paleoenvironmental distribution  
768 of microbialites during times of biotic crisis. *Geobiol* 10:3–24  
769 McGowan AJ, Smith AB, Taylor PD (2009) Faunal diversity, heterogeneity and body size in  
770 the Early Triassic: testing post-extinction paradigms in the Virgin Limestone of Utah,  
771 USA. *Aust J Earth Sci* 56:859–872  
772 Nielson RL (1991) Petrology, sedimentology and stratigraphic implications of the Rock  
773 Canyon Conglomerate, southwestern Utah. *Utah Geol Surv Misc Publ*:91–7  
774 Nielson RL, Johnson JL (1979) The Timpoweap Member of the Moenkopi Formation.  
775 Timpoweap Canyon, Utah: *Utah Geol* 6:17–27

776 Olivier N, Brayard A, Fara E, Bylund KG, Jenks JF, Vennin E, Stephen DA, Escarguel G  
777 (2014) Smithian shoreline migrations and depositional settings in Timpoweap Canyon  
778 (Early Triassic, Utah, USA). *Geol Mag* 151:938–955

779 Olivier N, Brayard A, Vennin E, Escarguel G, Fara E, Bylund KG, Jenks JF, Caravaca G,  
780 Stephen DA (2016) Evolution of depositional settings in the Torrey area during the  
781 Smithian (Early Triassic, Utah, USA) and their significance for the biotic recovery. *Geol J*  
782 51: 600–626

783 Paull RA, Paull RK (1993) Interpretation of Early Triassic nonmarine–marine relations, Utah,  
784 U.S.A. *N M Mus Nat Hist Sci Bull* 3:403–409

785 Paull RK, Paull RA (1994) Shallow marine sedimentary facies in the earliest Triassic  
786 (Griesbachian) Cordilleran miogeocline, USA. *Sediment Geol* 93:181–191

787 Paull RK, Paull RA (1997) Transgressive conodont faunas of the early Triassic: an  
788 opportunity for correlation in the Tethys and the circum-Pacific. In: *Late Palaeozoic and*  
789 *Early Mesozoic Circum-Pacific Events and their Global Correlation*, Dickins JM, Zunyi Y,  
790 Hongfu Y, Lucas SG, Acharyya SK (eds). Cambridge University Press, *World and*  
791 *Regional Geology* 10:158–167

792 Payne JL, Clapham ME (2012) End-Permian mass extinction in the oceans: an ancient analog  
793 for the twenty-first century? *Annu Rev Earth Planet Sci* 40:89–111

794 Payne JL, Lehrmann DJ, Wei J, Orchard MJ, Schrag DP, Knoll AH (2004) Large  
795 perturbations of the carbon cycle during recovery from the end-Permian extinction.  
796 *Science* 305:506–509

797 Payne JL, Lehrmann DJ, Wei J, Knoll AH (2006) The pattern and timing of biotic recovery  
798 from the end-Permian extinction on the Great Bank of Guizhou, Guizhou Province, China.  
799 *Palaios* 21:63–85

800 Payne, J. L., Turchyn, A. V., Paytan A, DePaolo DJ, Lehrmann DJ, Yu M, Wei J (2010)  
801 Calcium isotope constraints on the end-Permian mass extinction. *Proc Natl Acad Sci*  
802 107:8543–8548

803 Peng Y, Shi GR, Gao Y, He W, Shen S (2007) How and why did the Lingulidae  
804 (Brachiopoda) not only survive the end-Permian mass extinction but also thrive in its  
805 aftermath? *Palaeogeogr Palaeoclimatol Palaeoecol* 252:118–131

806 Pietsch C, Bottjer DJ (2014) The importance of oxygen for the disparate recovery patterns of  
807 the benthic macrofauna in the Early Triassic. *Earth Sci Rev* 137:65–84

808 Pietsch C, Mata SA, Bottjer DJ (2014) High temperature and low oxygen perturbations drive  
809 contrasting benthic recovery dynamics following the end-Permian mass extinction.  
810 *Palaeogeogr Palaeoclimatol Palaeoecol* 399:98–113

811 Pörtner HO, Langenbuch M, Michaelidis B (2005) Synergistic effects of temperature  
812 extremes, hypoxia, and increases in CO<sub>2</sub> on marine animals: From Earth history to global  
813 change. *J Geophys Res: Oceans*, 110(C9)

814 Posenato R, Holmer LE, Prinoth H (2014) Adaptive strategies and environmental significance  
815 of lingulid brachiopods across the late Permian extinction. *Palaeogeogr Palaeoclimatol*  
816 *Palaeoecol* 399:373–384

817 Pruss SB, Bottjer DJ (2004) Late Early Triassic microbial reefs on the western United States:  
818 a description and model for their deposition in the aftermath of the end-Permian mass  
819 extinction. *Palaeogeogr Palaeoclimatol Palaeoecol* 211:127–137

820 Pruss SB, Bottjer DJ, Corsetti FA, Baud A (2006) A global marine sedimentary response to  
821 the end-Permian mass extinction: Examples from southern Turkey and the western United  
822 States. *Earth Sci Rev* 78:193–206

823 Reeside Jr JB, Bassler H (1922) Stratigraphic sections in southwestern Utah and northwestern  
824 Arizona. *US Geol Surv Prof Papr* 129(D): 53–77

825 Ritter S, Osborn C, Goodrich C (2013) Sedimentology and reservoir characteristics of the  
826 Lower Triassic (Smithian) Sinbad Limestone Member of the Moenkopi Formation, San  
827 Rafael Swell, Utah. In: Morris TH, Renssetar R (eds) *The San Rafael Swell and Henry*  
828 *Mountains Basin—Geologic Centerpiece of Utah*. *Utah Geol Assoc Publ* 42:199–222

829 Rodland DL, Bottjer DJ (2001) Biotic recovery from the end-Permian mass extinction:  
830 behavior of the inarticulate brachiopod *Lingula* as a disaster taxon. *Palaios* 16:95–101

831 Schubert JK, Bottjer DJ (1992) Early Triassic stromatolites as post-mass extinction disaster  
832 forms. *Geology* 20:883–886

833 Schubert JK, Bottjer DJ (1995) Aftermath of the Permian-Triassic mass extinction event:  
834 paleoecology of Lower Triassic carbonates in the western USA. *Palaeogeogr*  
835 *Palaeoclimatol Palaeoecol* 116:1–39

836 Seilacher A (1963) Lebensspuren und Salinitätsfazies. *Fortschr Geol Rheinl Westfal* 10:81–  
837 94

838 Song H, Wignall PB, Chu D, Tong J, Sun Y, Song H, He W, Tian L (2014) Anoxia/high  
839 temperature double whammy during the Permian-Triassic marine crisis and its aftermath.  
840 *Sci rep*4:4132

841 Stewart JH, Poole FG, Wilson RF (1972) Stratigraphy and origin of the Triassic Moenkopi  
842 Formation and related strata in the Colorado Plateau region: U. S. Geol Surv Prof Pap  
843 691:195 p

844 Sun Y, Joachimski MM, Wignall PB, Yan C, Chen Y, Jiang H, Wang L, Lai X (2012)  
845 Lethally hot temperatures during the Early Triassic greenhouse. *Science* 338:366–370

846 Szmuc EJ, Osgood RG, Meinke DW (1977) Synonymy of the ichnogenus *Lingulichnites*  
847 Szmuc, E.J., Osgood, R.G., and Meinke, D.W. 1976, with *Lingulichnus* Hakes, 1976.  
848 *Lethaia* 10:106

849 Tang H, Kershaw S, Liu H, Tan X, Li F, Hu G, Huang C, Wang L, Lian C, Li L, Yang X  
850 (2017) Permian–Triassic boundary microbialites (PTBMs) in southwest China:  
851 implications for paleoenvironment reconstruction. *Facies* 63:2

852 Thomazo C, Vennin E, Brayard A, Bour I, Mathieu O, Elmeknassi S, Olivier N, Escarguel G,  
853 Bylund KG, Jenks J, Stephen DA, Fara E (2016) A diagenetic control on the Early Triassic  
854 Smithian–Spathian carbon isotopic excursions recorded in the marine settings of the  
855 Thaynes Group (Utah, USA). *Geobiol* 14:220–236 DOI: 10.1111/gbi.12174

856 Tomescu AM, Klymiuk AA, Matsunaga KK, Bippus AC, Shelton GW (2016) Microbes and  
857 the Fossil Record: Selected Topics in Paleomicrobiology. In: *Their World: A Diversity of*  
858 *Microbial Environments* (pp. 69-169). Springer International Publishing

859 Twitchett RJ, Krystyn L, Baud A, Wheeley JR, Richo S (2004) Rapid marine recovery after  
860 the end-Permian mass-extinction event in the absence of marine anoxia. *Geology* 32:805–  
861 808

862 Vennin E, Olivier N, Brayard A, Bour I, Thomazo C, Escarguel G, Fara E, Bylund KG, Jenks  
863 JF, Stephen DA, Hofmann R (2015) Microbial deposits in the aftermath of the end-  
864 Permian mass extinction: a diverging case from the Mineral Mountains (Utah, USA).  
865 *Sedimentol* 62:753–792

866 Wignall PB, Twitchett RJ (1996) Oceanic anoxia and the end Permian mass extinction.  
867 *Science* 272:1155

868 Woods AD (2014) Assessing Early Triassic paleoceanographic conditions via unusual  
869 sedimentary fabrics and features. *Earth Sci Rev* 137:6–18

870 Yang H, Chen ZQ, Wang Y, Tong J, Song H, Chen J (2011) Composition and structure of  
871 microbialite ecosystems following the end-Permian mass extinction in South China.  
872 *Palaeogeogr Palaeoclimatol Palaeoecol* 308:111–128

873 Yang H, Chen ZQ, Wang Y, Ou W, Liao W, Mei X. (2015) Palaeoecology of microconchids  
874 from microbialites near the Permian–Triassic boundary in South China. *Lethaia* 48:497–  
875 508

876 Zonneveld JP, Pemberton SG (2003) Ichnotaxonomy and behavioral implications of  
877 lingulide-derived trace fossils from the Lower and Middle Triassic of Western Canada.  
878 *Ichnos* 10:25–39

879 Zonneveld JP, Beatty TW, Pemberton SG (2007) Lingulide brachiopods and the trace fossil  
880 *Lingulichnus* from the Triassic of western Canada: implications for faunal recovery after  
881 the end-Permian mass extinction. *Palaios* 22:74–97

882  
883  
884  
885  
886  
887

888 **Figure captions**

889  
890

891 **Fig. 1 a** Present-day location of the study area in southwestern Utah, along the Hurricane  
892 Cliffs, about 8 km south of Hurricane city. **b** Early Triassic paleogeographic map showing the  
893 location of southwestern USA along the Pangea margin (after Brayard et al. 2013)

894

895 **Fig. 2 a** Field view of section #1 on the western side of the Hurricane Cliffs (see geographic  
896 location on Fig. 1a) showing the Permian-Triassic transition. The studied outcrop is about 70  
897 m thick. **b** Field view of the eastern side of the Hurricane Cliffs, just south of the Three  
898 Brothers Tertiary volcanic peaks. Sections #2-5 were logged along the head end of Workman  
899 Wash. Geologists near section #5 for scale

900

901 **Fig. 3** Legend for Figures 4-8 and 15

902

903 **Fig. 4** Log of the studied interval on the western side of the Hurricane Cliffs. See location on  
904 Figures 1a and 2, Table 1 for facies descriptions, and Figure 3 for legend

905

906 **Fig. 5** Log of section #2. See location on Figures 1a and 2b, Table 1 for facies descriptions,  
907 and Figure 3 for legend

908

909 **Fig. 6** Log of section #3. See location on Figures 1a and 2b, Table 1 for facies descriptions,  
910 and Figure 3 for legend

911

912 **Fig. 7** Log of section #4. See location on Figures 1a and 2b, Table 1 for facies descriptions,  
913 and Figure 3 for legend

914

915 **Fig. 8** Log of section #5. See location on Figures 1a and 2b, Table 1 for facies descriptions,  
916 and Figure 3 for legend

917

918 **Fig. 9** Field illustrations of some facies and macroorganisms. **a** Fenestral-microbial facies  
919 (F7). The lower part of the picture shows a macroscopic laminated microbial structure  
920 whereas the upper part displays a fenestral fabric (subfacies F7b; section #1, about 52 m). **b**  
921 Fenestral-microbial limestones (F7) with large fenestrae and endostromatolites (subfacies  
922 F7b; section #2, about 4 m). **c** Accumulation of large-sized gastropods (subfacies F7b; section  
923 #4, about 3 m). **d** Accumulation of ammonoids (subfacies F7c; section #5, about 6 m). **e**  
924 Intensively bioturbated interval corresponding to the marker bed with lingulid brachiopods  
925 (Facies F11; section #4, about 4.5 m). **f** Conglomerate breccia (Facies F1; base of section #4).  
926 **g** Yellow clastic unit (Facies F5; section #4, about 15 m)

927

928 **Fig. 10 a** Field view and **b** cartoon of the fenestral-microbial facies (F7) locally showing  
929 reefal morphology and truncation surfaces above the lingulid marker bed

930

931 **Fig. 11** Natural-light thin-section photographs of the fenestral-microbial facies (F7). **a** Oo-  
932 pisoid subfacies F7a with pisoids (sometimes truncated), ooids and peloids in a sparitic  
933 cement. **b** Intraclastic subfacies F7e with abundant intraclasts in a sparitic cement. **c-f**  
934 Fenestral-limestone subfacies F7b with various types of endostromatolites. **c** Thin crusts of  
935 dense micrite with downward or upward growth directions at the roof and the floor of a  
936 fenestrae. **d** Coalescent stromatolitic columns with a marked lamination, which locally  
937 displays some putative residual calcified sheaths of filamentous bacteria (arrows). **e** Complex  
938 crust made of an alternation of sparitic and micritic laminae. **f** Acicular to botryoidal cements  
939 associated with a lamination of an endostromatolites in a large fenestrae. **g** Subfacies F7c with

940 an interval made of domal to columnar stromatolites, topped by a lamellar siliceous sponge. **h**  
941 Lamellar siliceous sponge (subfacies F7c)

942

943 **Fig. 12** Natural-light thin-section photographs of the fenestral-microbial facies (F7). **a** Root  
944 structures and circum-granular cracks, subfacies F7c. **b** Subfacies F7d with small fenestrae  
945 and abundant extraclasts. **c** Biofilm (white arrow) coating a pel-fenestral structure, subfacies  
946 F7c. **d** Biofilms coating a peloidal grainstone above an oncoidal-fenestral structure, subfacies  
947 F7c. **e** Biofilms coating a peloidal grainstone above a micritic stromatolite, subfacies F7c. **f** A  
948 stromatolitic crust displaying a columnar microfabric, subfacies F7c. **g** Planar to wavy  
949 structure of a stromatolite, subfacies F7c. **h** Enigmatic cemented crust, subfacies F7c

950

951 **Fig. 13** Natural-light thin-section photographs of the bioclastic facies. **a** Spicule-echinoderm  
952 limestone (F9). Note the common echinoderm fragments (white arrows) and the darker (more  
953 micritic) areas reflecting a probable infaunal activity. **b** Oo-pel-bioclastic limestone (F10). **c**  
954 Pel-bioclastic limestone (F12). **d** Intra-bioclastic limestone (F13)

955

956 **Fig. 14** Lingulid brachiopods in Facies F11, section #4, about 8 m (see Figure 2b and 7). **a** In-  
957 situ large complete shell of *Lingularia* in life position characterizing the marker bed attributed  
958 to facies F11 at Workman Wash. **b** Typical example of *Lingulichnus verticalis* associated to  
959 lingulid shells in facies F11. Note the pedicle trace and the set of downward-deflected  
960 laminae produced by upward adjustment of the lingulid in response to sediment aggradation  
961 (equilibration structure). Scale bar (valid for both photographs) is 5 mm

962

963 **Fig. 15** Correlation of sections. See figures 1 and 2 for their location

964

965 **Fig. 16** Schematic 3D reconstruction of the depositional setting for the late Smithian  
966 sedimentary rocks observed at Workman Wash

967

968 **Table 1** Facies description and depositional environments

Figure01

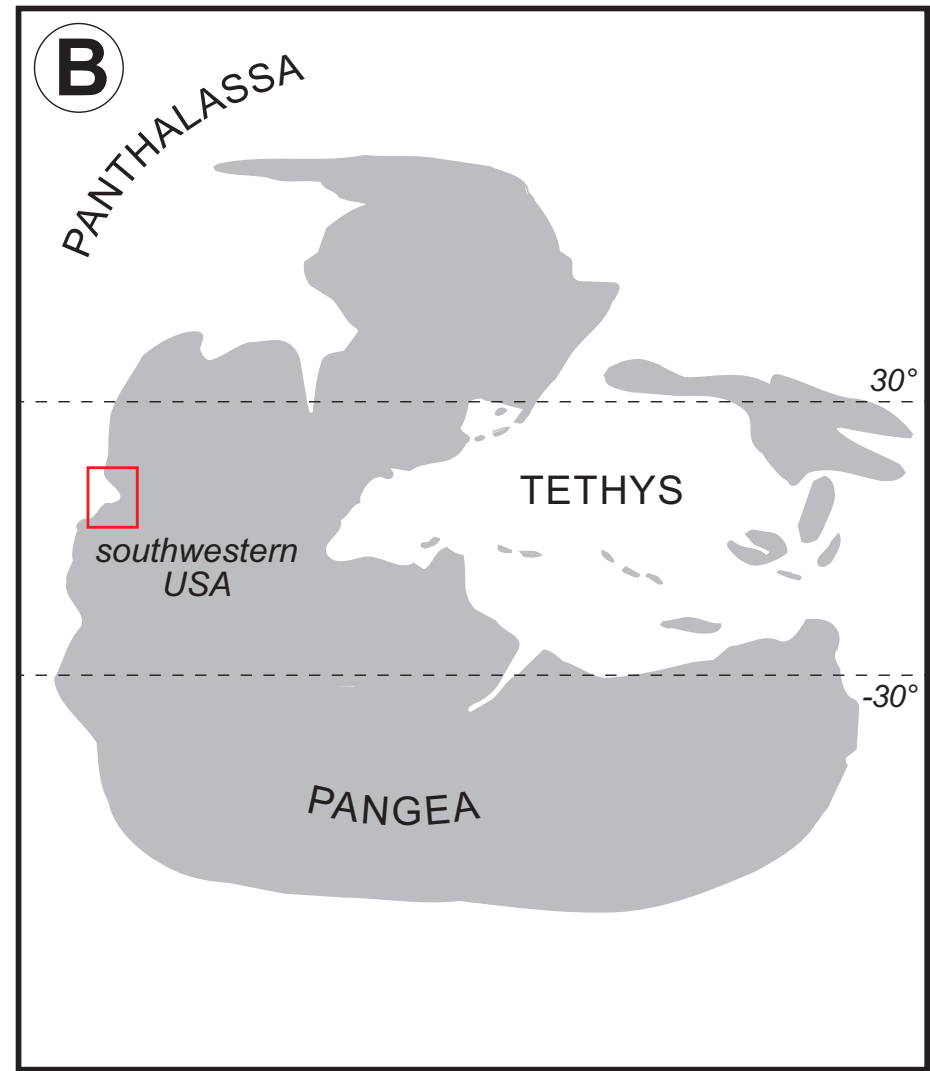
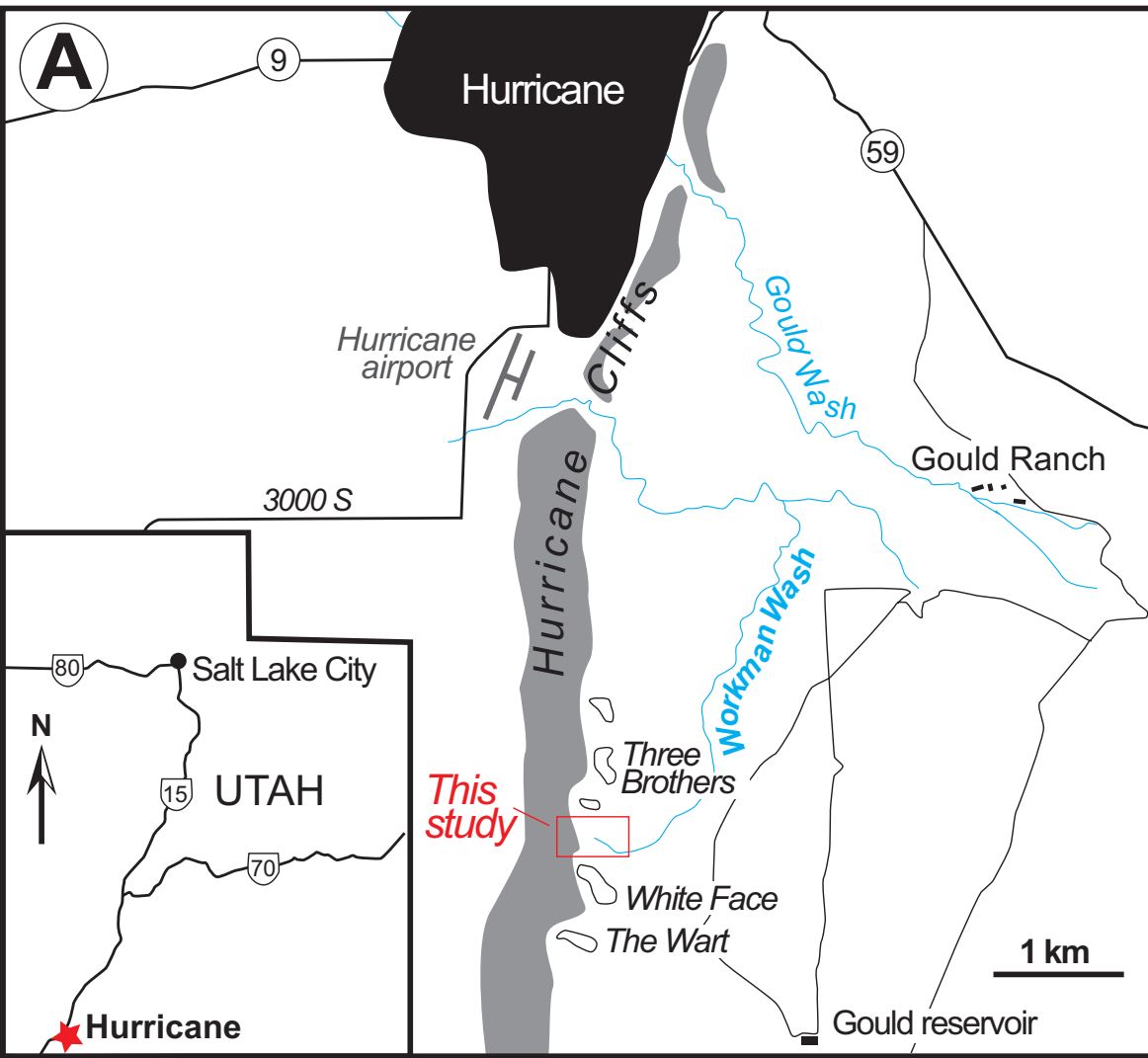


Figure02



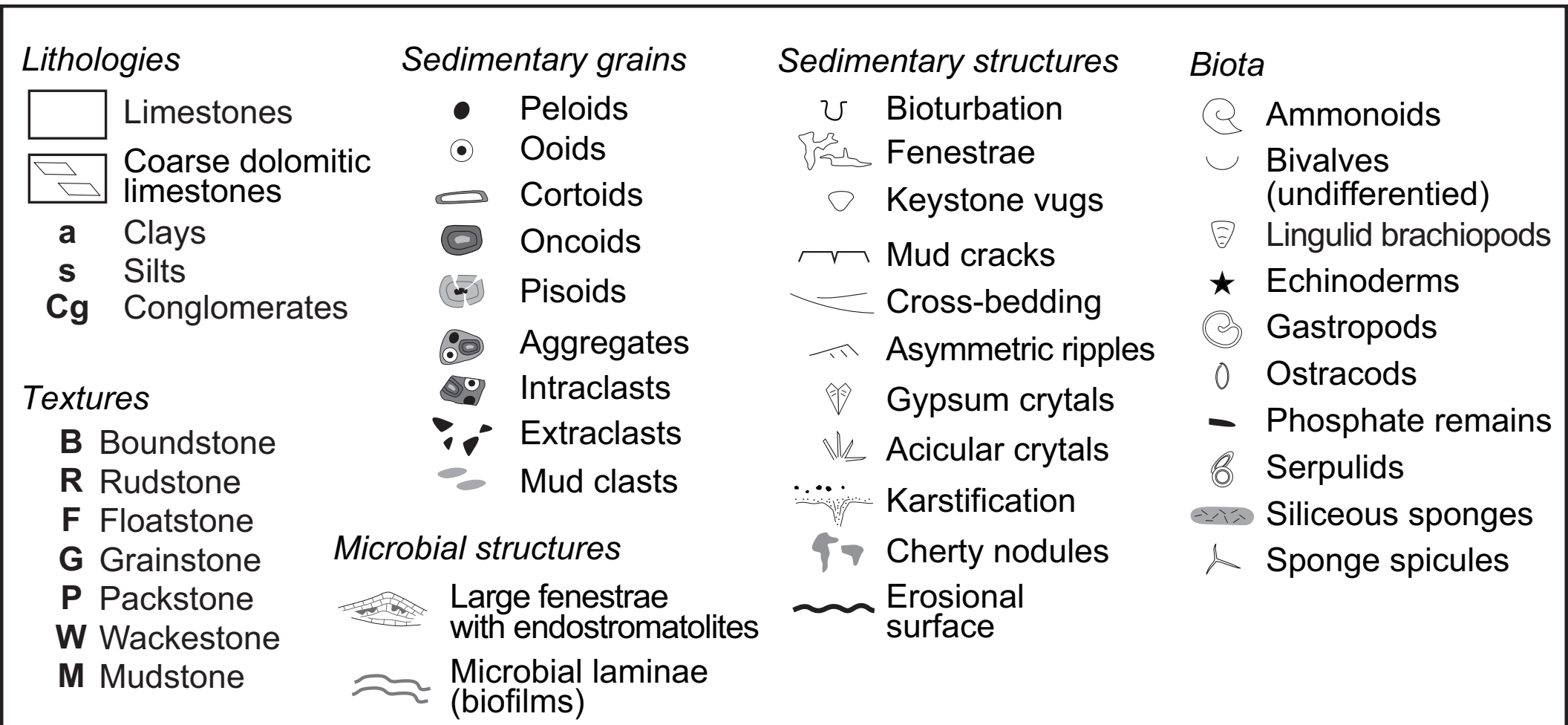




Figure04suite

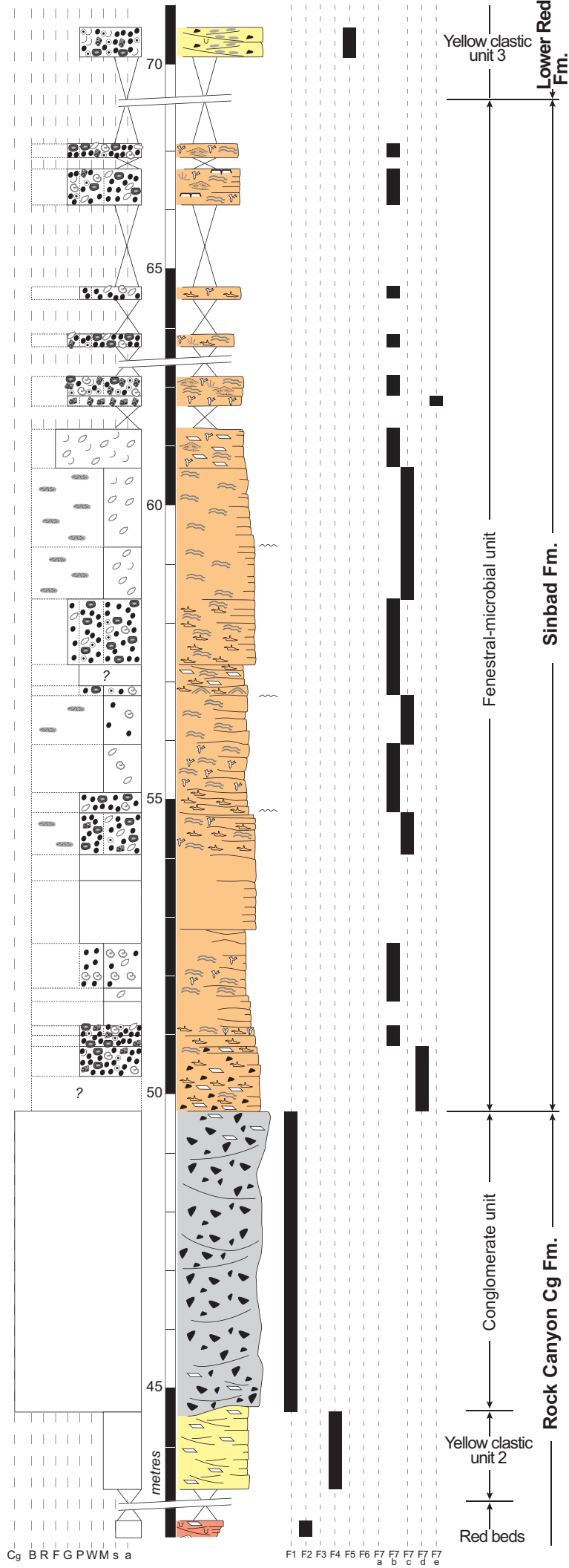


Figure05

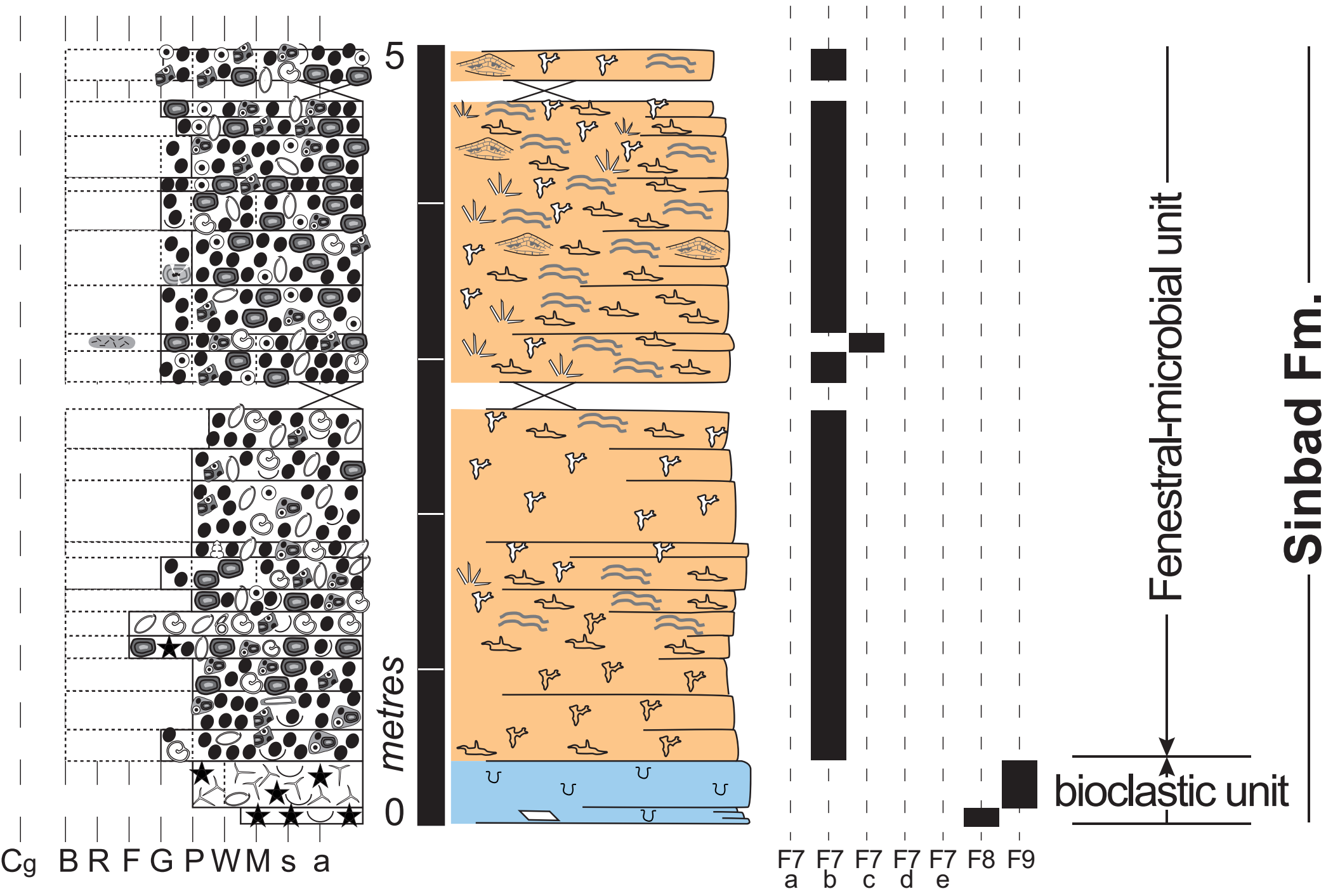


Figure06

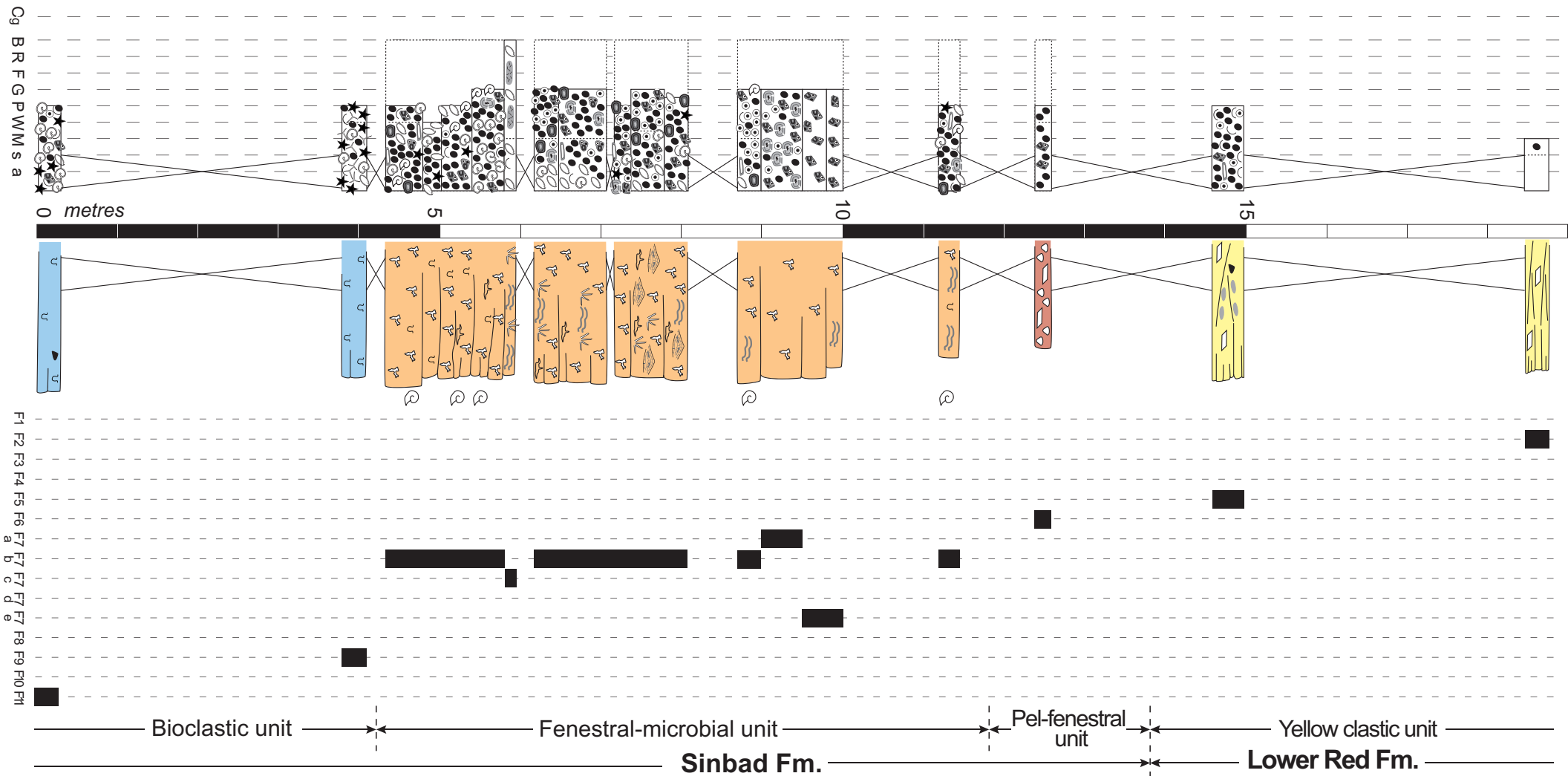
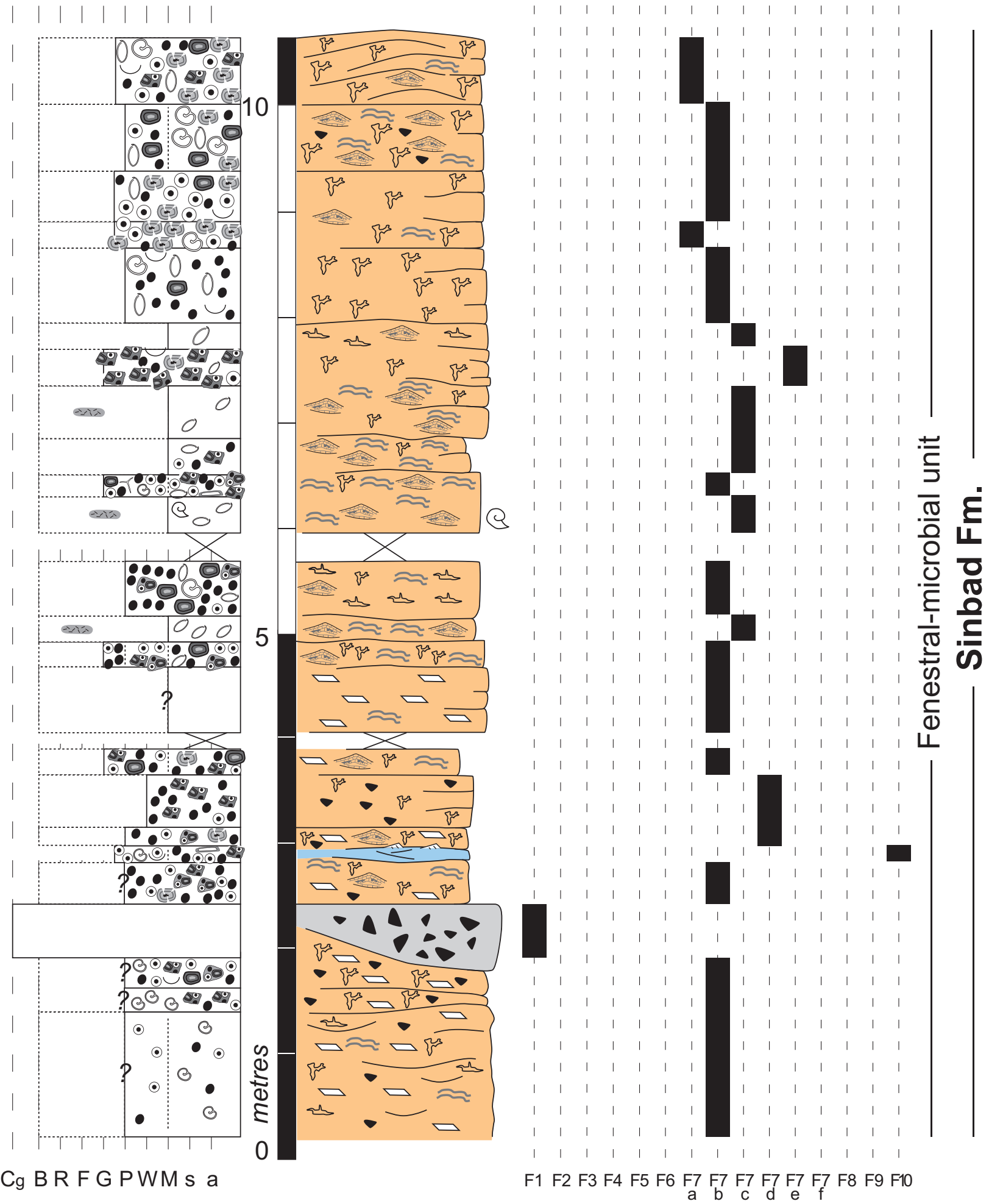




Figure08



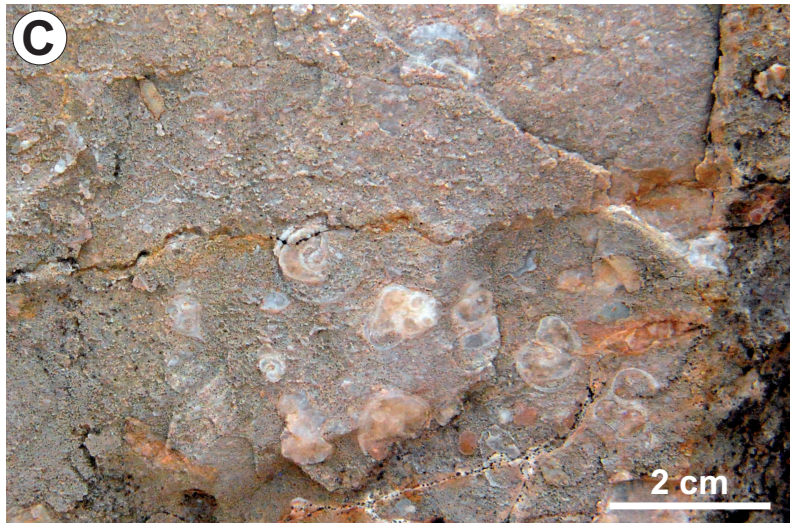


Figure 10 revised

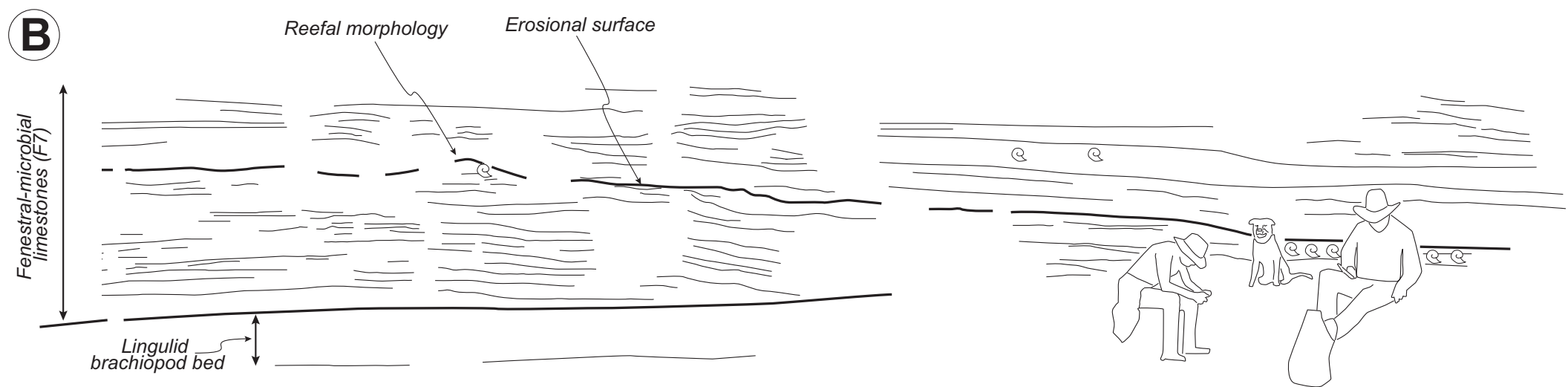


Figure 11

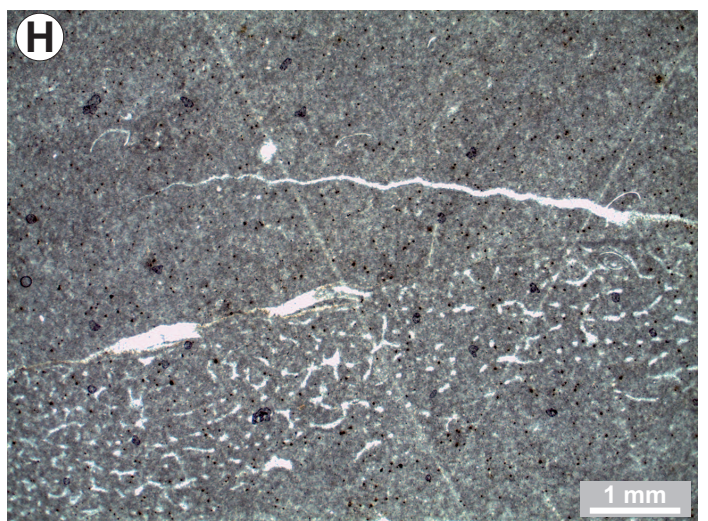
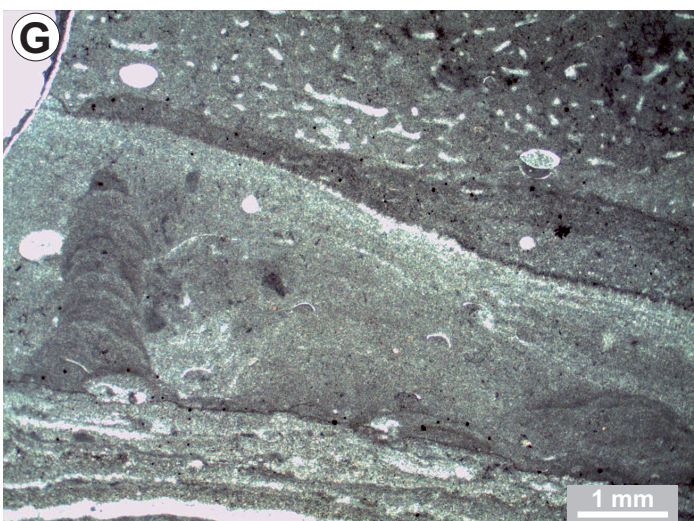
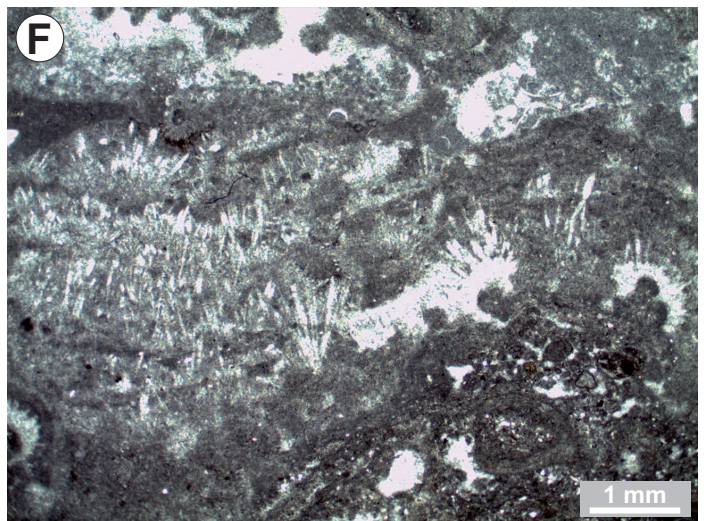
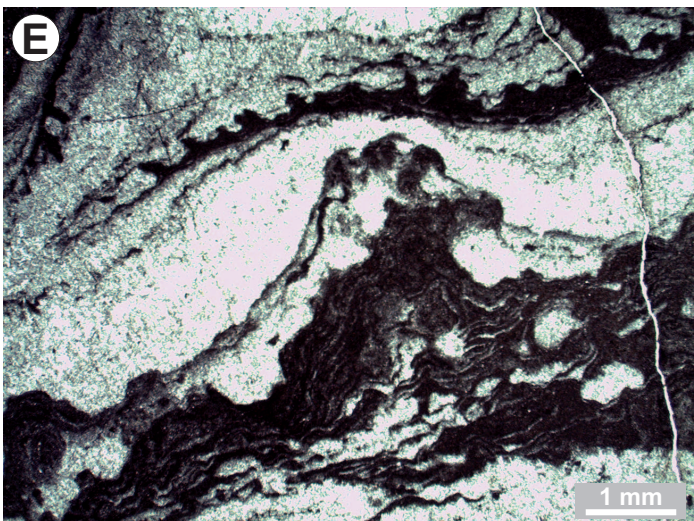
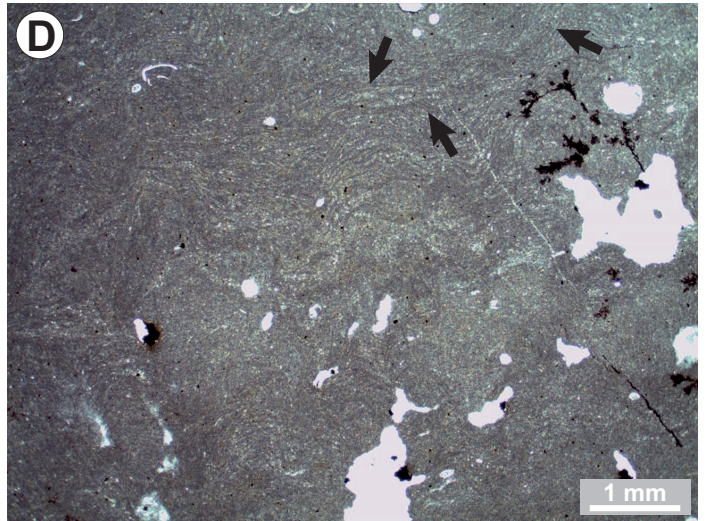
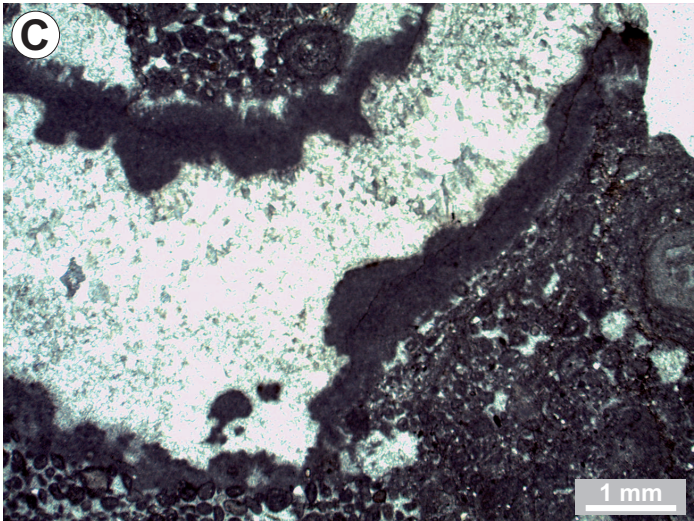
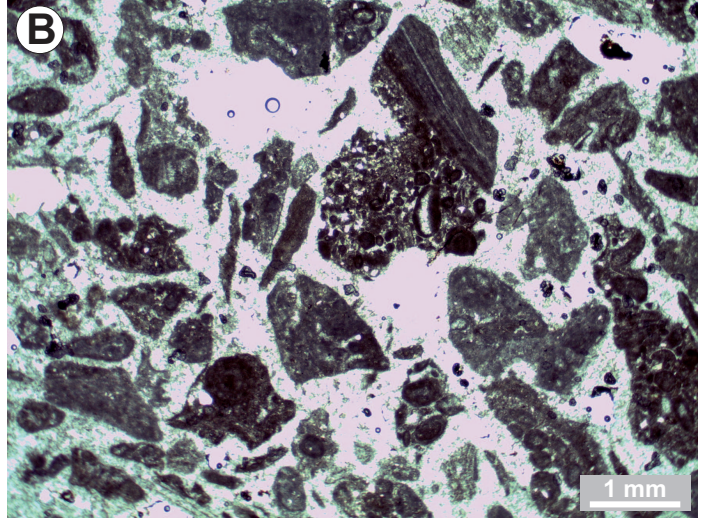
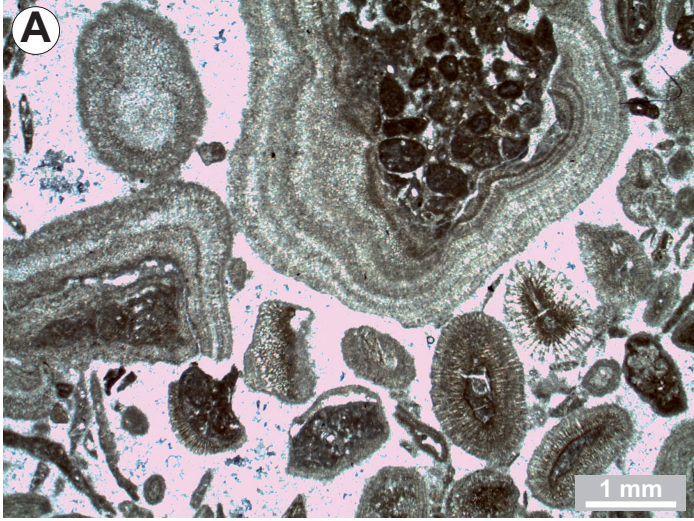
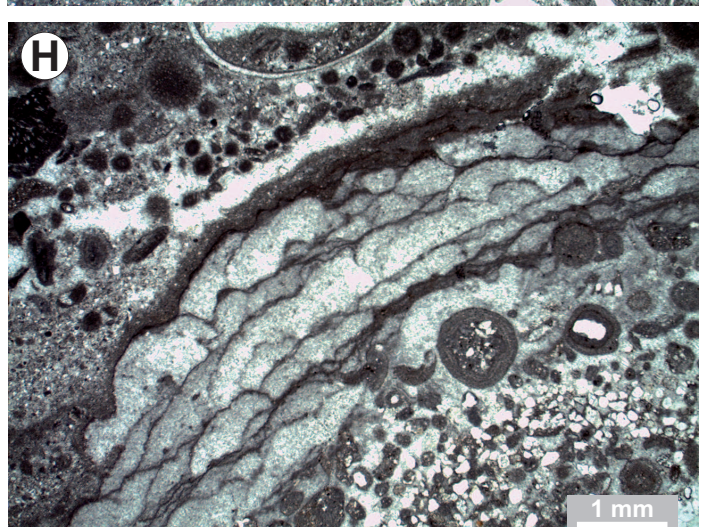
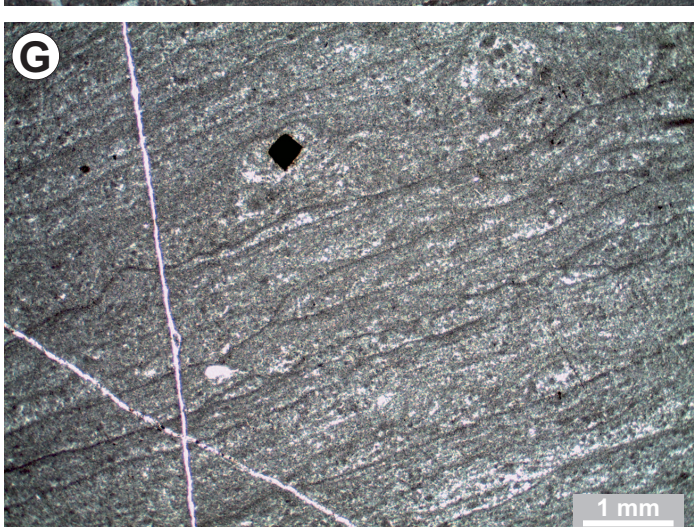
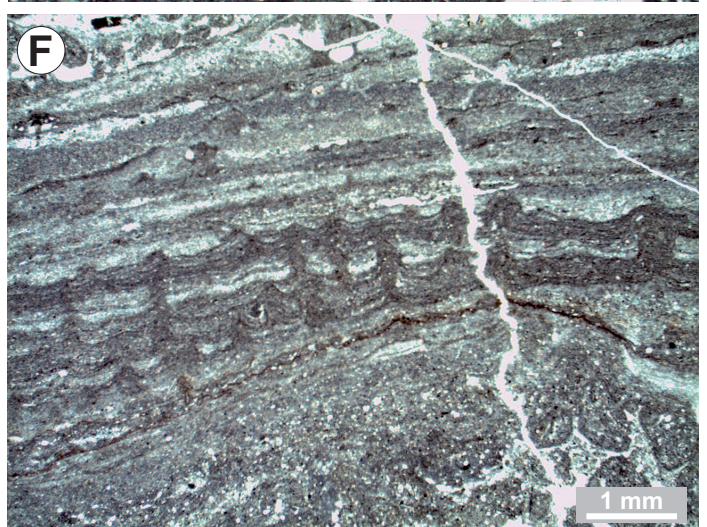
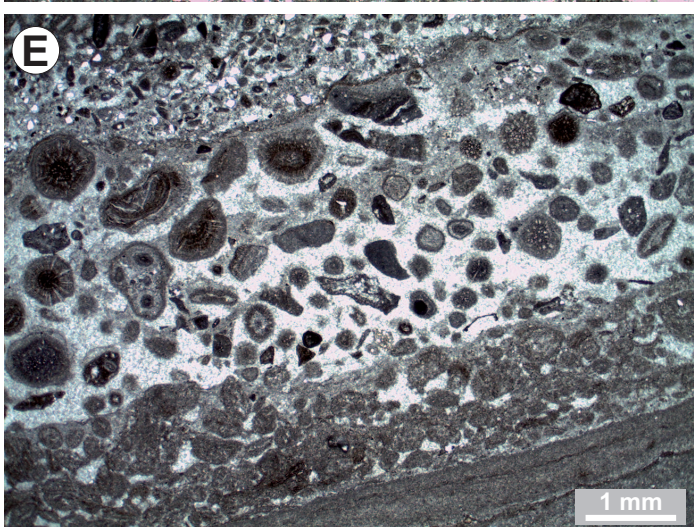
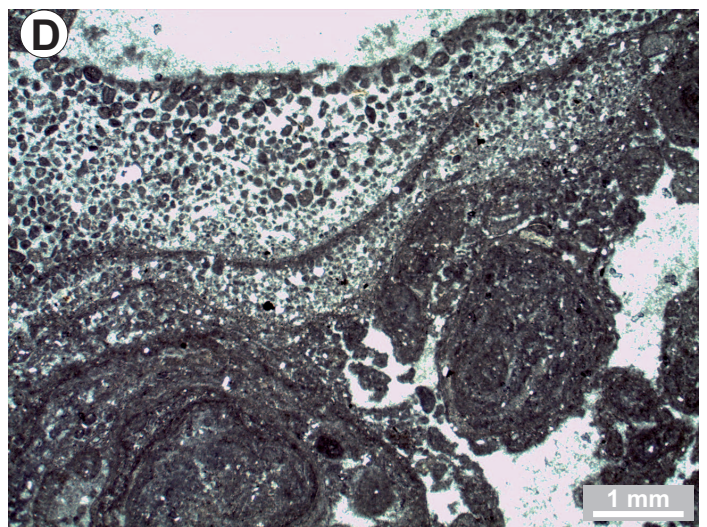
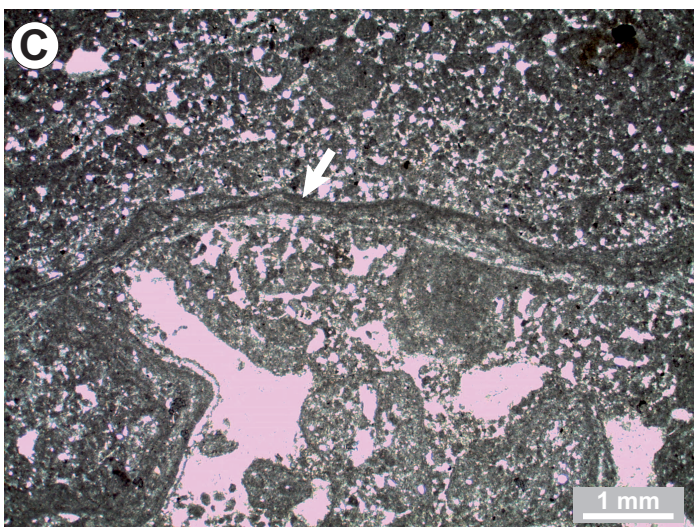
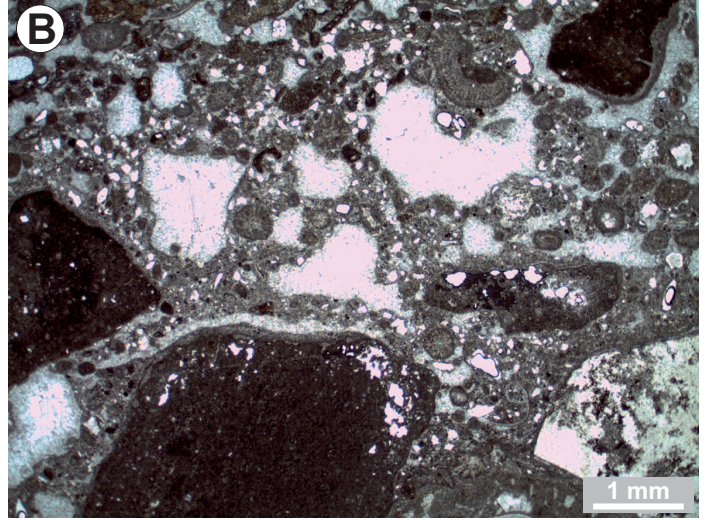


Figure 12



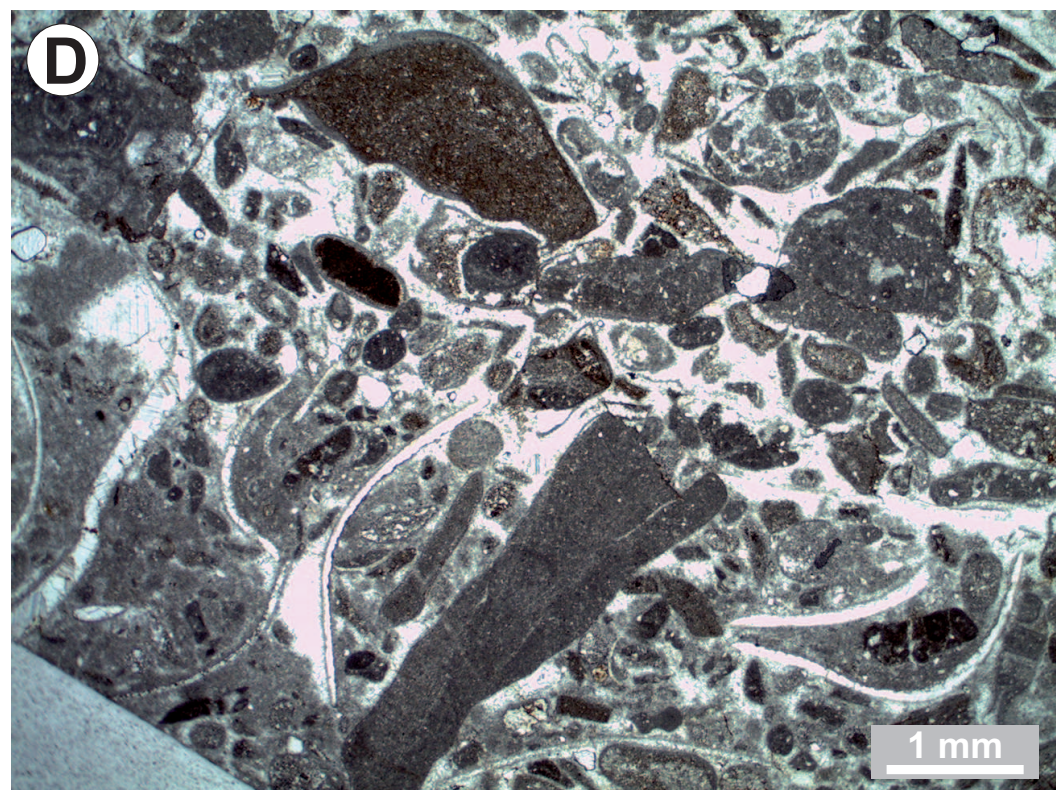
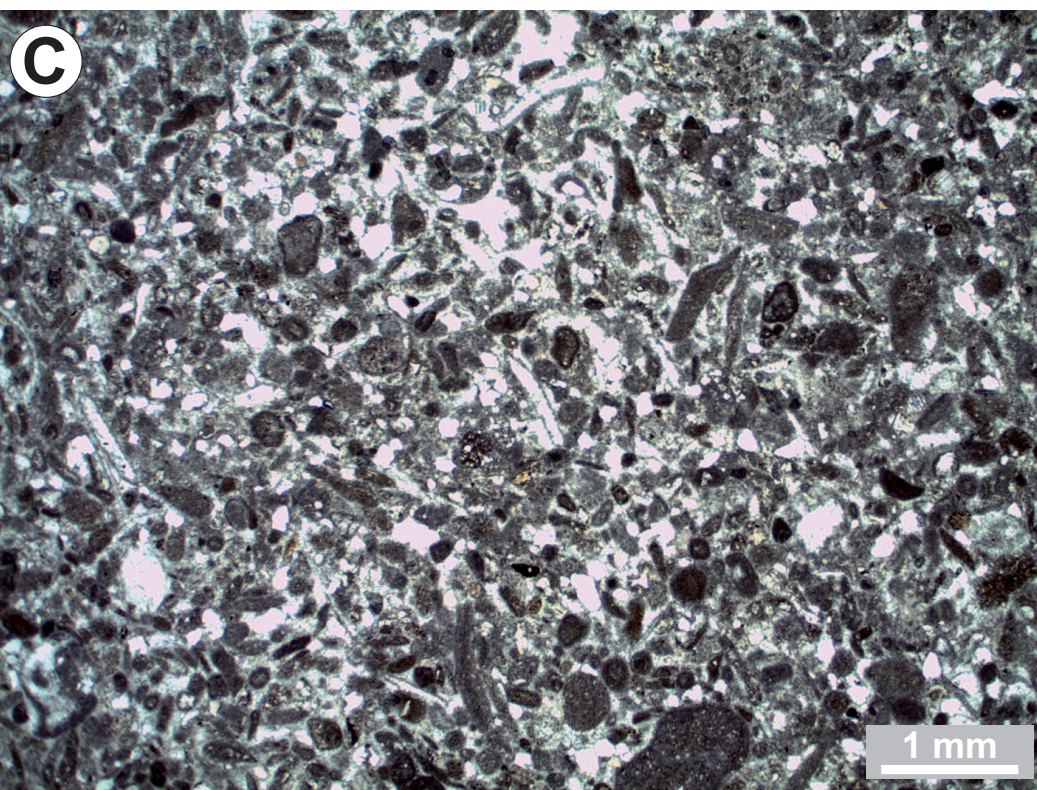
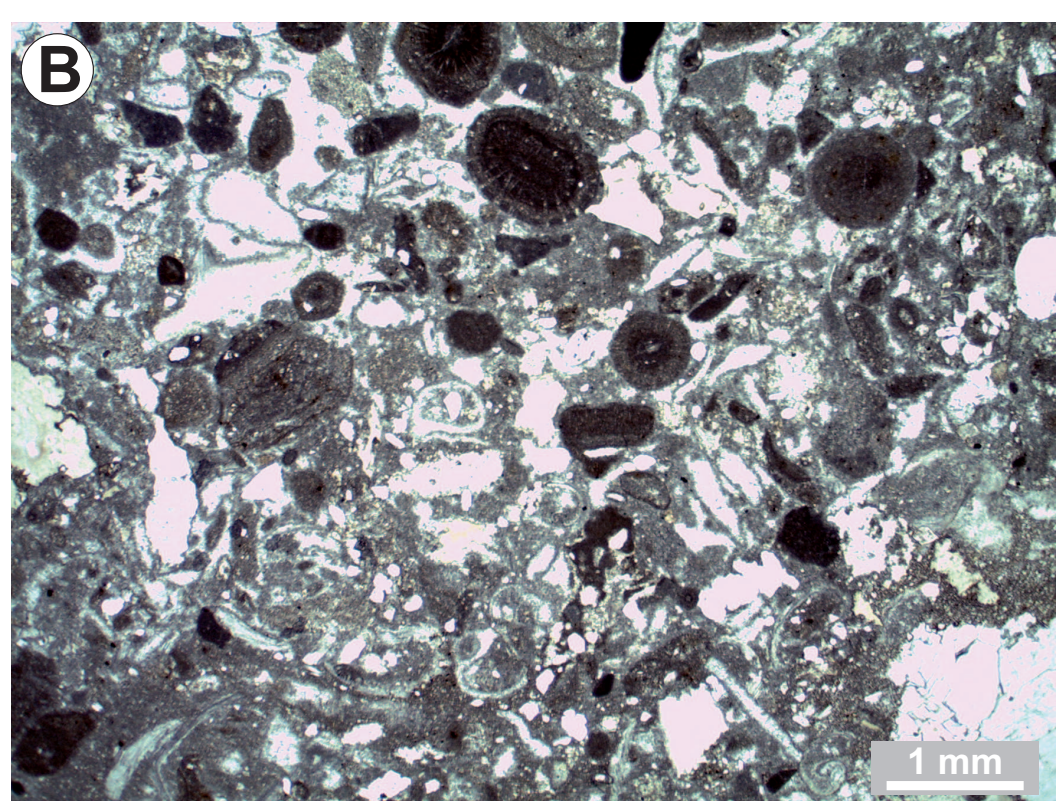
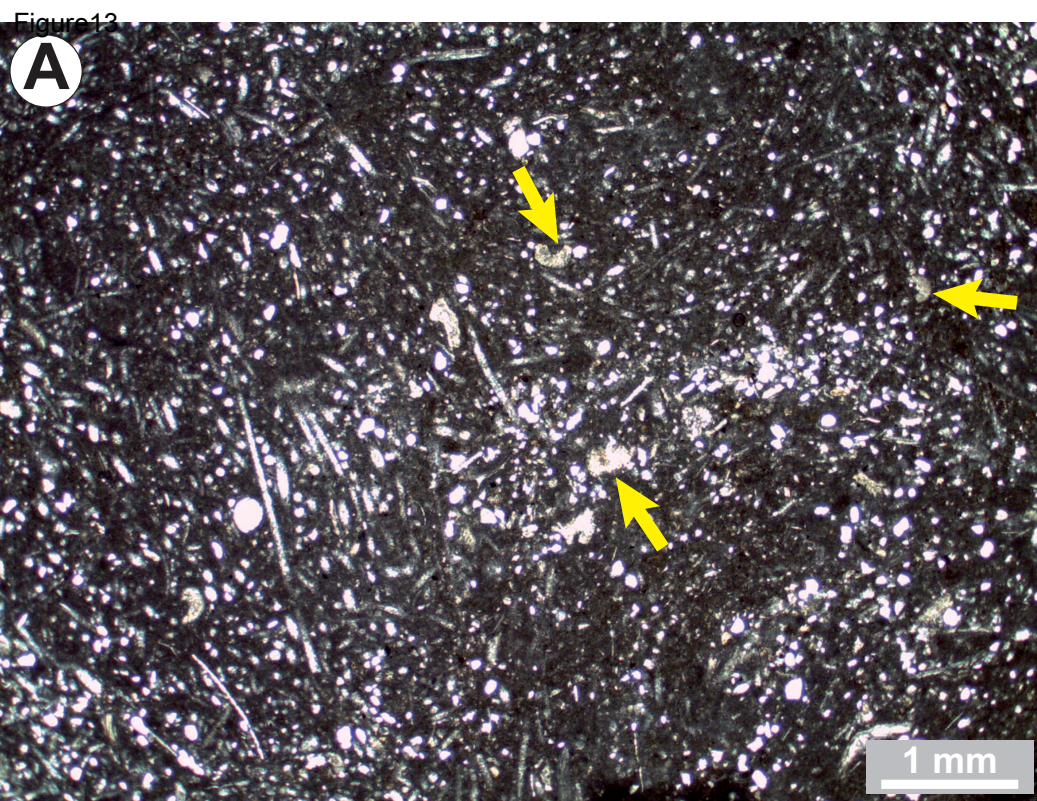


Figure14



Figure 15

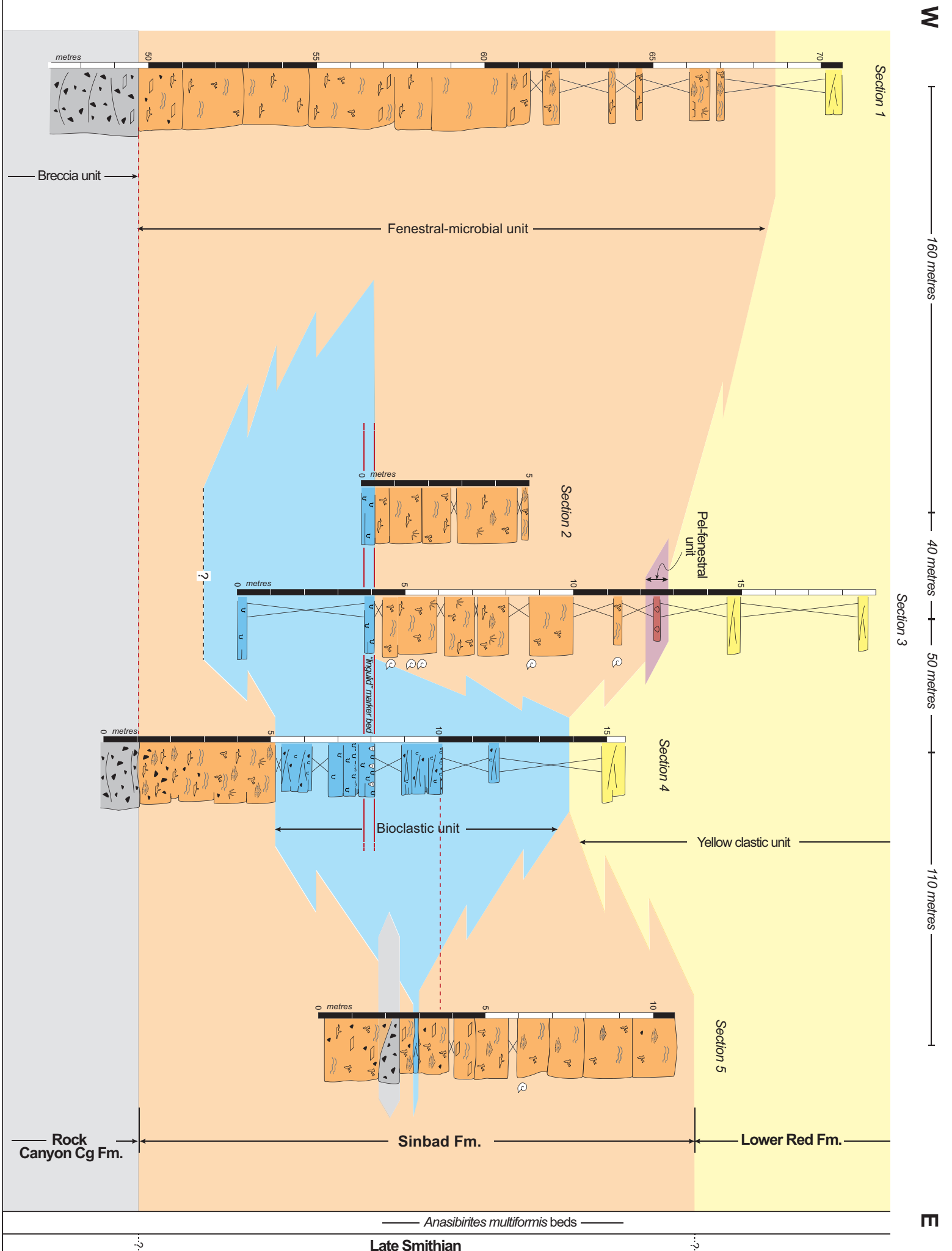


Figure 16

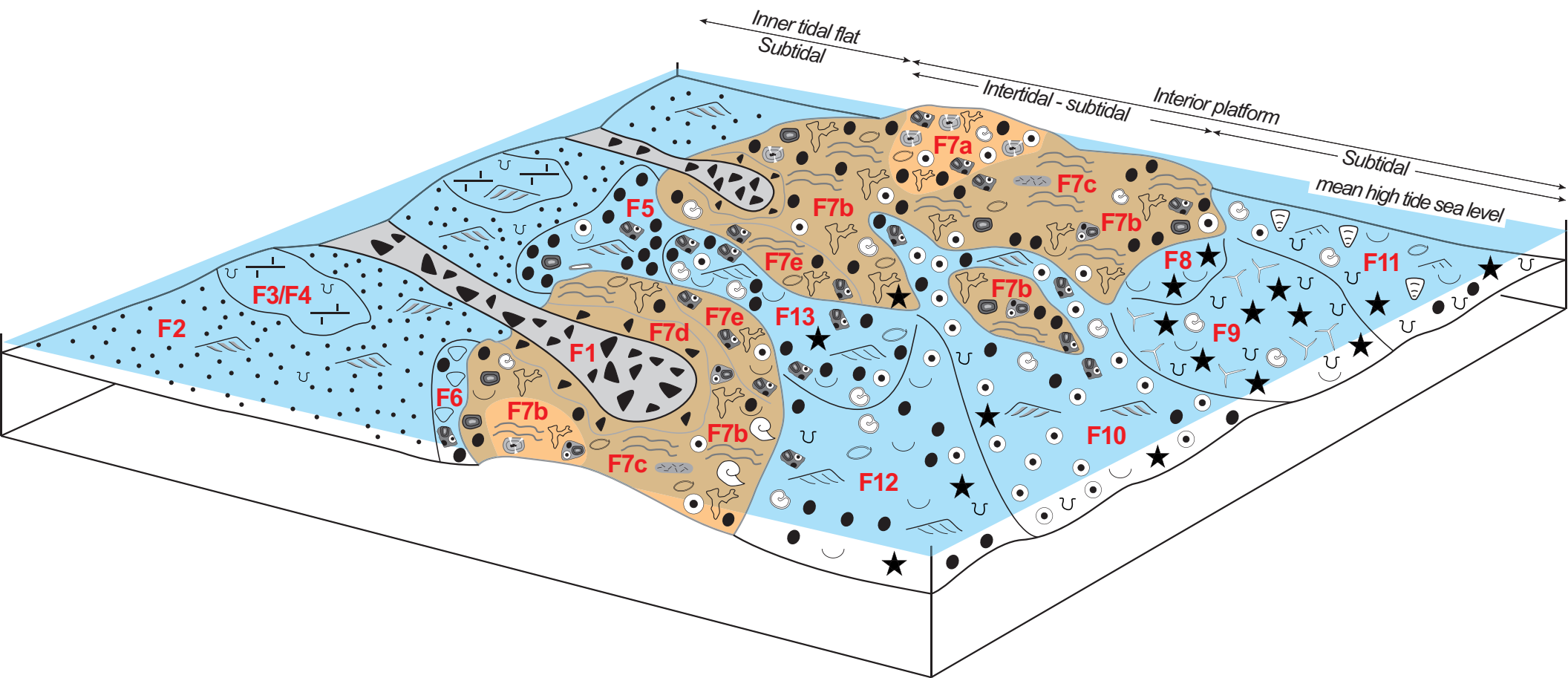


Table01

Facies		Textures	Biotic/non biotic grains	Matrix/cements	Sedimentary structures	Zones	Environments	
<b>F1</b>	Conglomerate breccia	—	Polygenic clasts (cherts, bioclastic limestones, red beds), with diameter up to 15 cm (commonly elongated). Poorly sorted and angular to subrounded clasts.	Silty matrix	Stacked and amalgamated channel complexes (with individual channel up to 2 m large and 1.3 m thick). Locally, some m-scale isolated channels.	Peritidal (subtidal)	Chennalized inner tidal flat	
<b>F2</b>	Dolosiltstone	—	Common peloids. Abundant well sorted and subangular to subrounded quartz grains.	Dolomitized micritic matrix	Trough cross bedding and asymmetrical ripples. Mud drapes. Common bioturbation.		Inner tidal flat	
<b>F3</b>	Dolomudstone	M	—	Dolomitized micritic matrix	Trough cross bedding with low angle foresets. Asymmetrical ripples. Common bioturbation.			
<b>F4</b>	Dolostone	—	—	Dolomitic cement	—			
<b>F5</b>	Silty peloidal limestone	P	Frequent to rare bivalves. Rare gastropods. Abundant peloids. Frequent to common micritized ooids. Common cortoids and intraclasts. Rare oncooids. Rounded to subrounded mudclasts.	Dolomitized micritic matrix	Trough cross bedding with low angle fore sets. Mud drapes and mud clasts. Rare extraclasts. Surimposed asymmetrical ripples. Common to rare bioturbation.			
<b>F6</b>	Keystone vug limestone	P/W	Frequent peloids, common micritic and microbial (reworked?) clasts.	Dolomitized micritic matrix	Frequent keystone vugs. Rare bioturbation.	Swash	Interior platform	
<b>F7</b>	Fenestral-microbial limestone	<b>F7a</b>	Oo-pisoid limestone	R(G/P)/B	Abundant ooids. Abundant to common pisoids and intraclasts. Frequent to common peloids. Rare (fragmented) gastropods and ostracods.	Micritic matrix/sparitic cement		Abundant small fenestra. Some large fenestrae with endostromatolites. Locally, some vadose silt. Sparse microbial laminae.
		<b>F7b</b>	Fenestral-limestone	P(G,W)/F/B(M)	Frequent to rare ostracods. Locally, frequent ammonoids. Abundant to rare gastropods. Frequent to rare bivalves. Rare echinoderms. Abundant to frequent peloids. Abundant to rare ooids. Common oncooids and intraclasts. Common to rare cortoids and pisoids.	Sparitic cement/micritic matrix/acicular crystals		Abundant small fenestrae. Locally large fenestrae (with upward and downward growth stromatolitic crusts). Mud cracks and vadose silt. Common microbial laminae. Rare bioturbation (?).
		<b>F7c</b>	Sponge-microbial limestone	B	Common ostracods and sponges. Rare bivalves.	Micritic laminae. Acicular crystals		Stromatolites (micritic lamination). Locally, some root structures and circum-granular cracks.
		<b>F7d</b>	Conglomerate limestone	B/P-M	Frequent to rare gastropods and ostracods. Rare bivalves. Frequent to rare peloids and ooids. Rare intraclasts and oncooids. Abundant extraclasts (polygenic, poorly sorted, elongated up to 7 cm long).	Micritic matrix		Abundant thin, elongated and aligned fenestrae or large fenestrae with endostromatolites. Sparse microbial laminae.
		<b>F7e</b>	Intraclastic limestone	G/B	Abundant intraclasts (fragmented pisoidal, ooidal, and peloidal clasts). Rare bivalves, ostracods, and gastropods.	Sparitic cement		Frequent fenestrae. Rare microbial laminae (and bioturbation?).
<b>F8</b>	Echinoderm dolomicrite	W	Frequent echinoderms. Common to rare bivalves. Rare gastropods.	Dolomitized micritic matrix	Sparse bioturbation.	Subtidal (tide dominated)		
<b>F9</b>	Spicule-echinoderm limestone	P(W)	Abundant echinoderms. Frequent sponge spicules, bivalves, and gastropods. Common ostracods. Rare phosphate remains. Common peloids.	Micritic matrix	Abundant bioturbation.			
<b>F10</b>	Oo-pel-bioclastic limestone	P	Abundant gastropods. Frequent bivalves. Common echinoderms. Abundant ooids. Common peloids. Rare intraclasts	Micritic matrix	Trough cross bedding with low angle foresets. Some mud drapes and mud clasts. Frequent bioturbation.			
<b>F11</b>	Bioturbated and bioclastic limestone	P	Abundant to rare echinoderms. Abundant to frequent gastropods and bivalves. Common to rare ostracods. Frequent to rare phosphate remains. Some lingulid brachiopods. Frequent to rare peloids. Rare ooids.	Micritic matrix	Abundant bioturbation ( <i>Arenicolites</i> , <i>Thalassinoides</i> , and <i>Paleoptycus</i> ). Some small asymmetrical ripples.			
<b>F12</b>	Pel-bioclastic limestone	G/P	Frequent bivalves. Frequent to common gastropods. Frequent to rare echinoderms. Rare ostracods and phosphatic remains. Abundant peloids. Common to rare ooids. Rare intraclasts.	Micritic matrix/sparitic cement	Trough cross bedding with low angle foresets. Small erosive channel with lateral accretion. Frequent to common bioturbation.			
<b>F13</b>	Intra-bioclastic limestone	G(P)	Frequent gastropods and bivalves. Rare echinoderms, ostracods, and phosphatic remains. Abundant peloids. Frequent intraclasts. Common ooids.	Sparitic cement	Trough cross bedding with low angle foresets.			